Electronic supporting information

for

Optimization of selectivity and rate of copper radioisotopes complexation: Formation and dissociation kinetic studies of 1,4,8-trimethylcyclam-based ligands with different coordinating pendant arms

Monika Paúrová,[a] Tomáš David,[a] Ivana Císařová,[a] Přemysl Lubal,[b] Petr Hermann [a] and Jan Kotek *[a]

---

[a] *Department of Inorganic Chemistry, Faculty of Science, Charles University, Hlavova 8, 128 43 Prague 2, Czech Republic. Tel.: +420221951436; fax: +420221951253; e-mail: modrej@natur.cuni.cz.*

[b] *Department of Chemistry, Faculty of Science, Masaryk University, Kotlářská 2, 611 37, Brno, Czech Republic.*

Table of contents

Details of refinement of the crystal structures

In the structure of $H_2\mathbf{L^3}\cdot H_2O$, no disorder was found. Hydrogen atoms bound to heteroatoms were fixed in original position as their full refinement led to too long bond distances, probably due to their involvement in strong hydrogen bonds. In the structure of $Li[Cu(\mathbf{L^5})](NO_3)\cdot 3H_2O$, no disorder was found. Hydrogen atoms bound to oxygen atoms were fully refined. In the structure of $\{Cu(H_2O)_2[Cu(\mathbf{L^7})]\}(ClO_4)\cdot 2H_2O\cdot 0.5$acetone, no disorder was found. Hydrogen atoms bound to oxygen atoms were fixed in original positions. Acetone molecule was found to be located very close to the inversion centre, and, thus, its occupancy was fixed to 0.5 to avoid space-conflict of atoms. In the structure of $\{Cu[Cu(\mathbf{L^{10}})]_2\}\cdot 19H_2O$, one of water molecules of crystallization was best refined disordered in two positions, with both parts sharing one of hydrogen atoms. Hydrogen atoms bound to oxygen atoms were fixed in original positions to keep a number of refined parameters low.

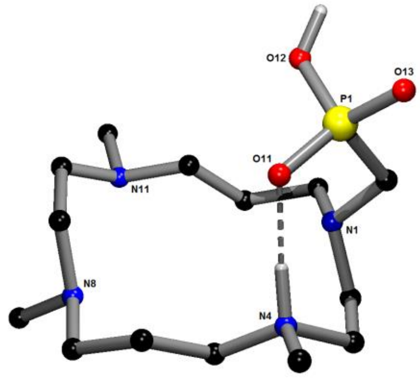

Figure S1. Molecular structure of $H_2\mathbf{L^3}$ found in the crystal structure of $H_2\mathbf{L^3}\cdot H_2O$. Carbon-bound hydrogen atoms are not shown. Colour code: P: yellow; O: red, N: blue, C: black, H: white.

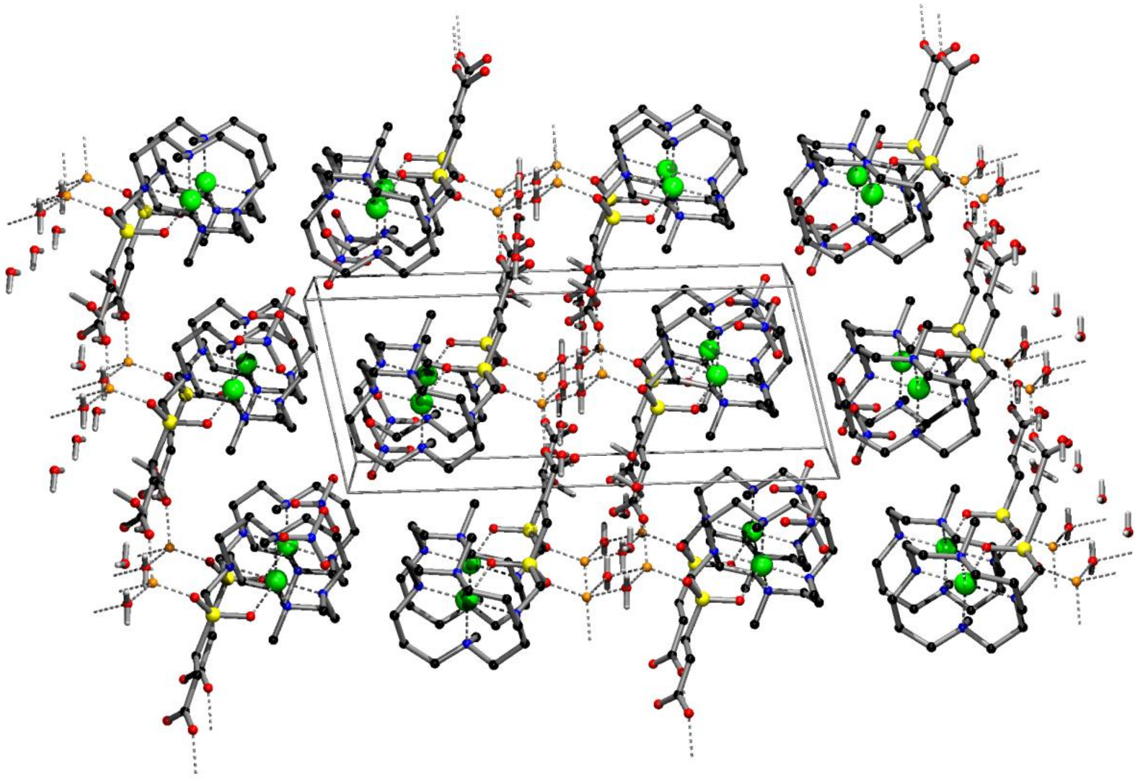

Figure S2. Crystal packing found in crystal structure of $Li[Cu(\mathbf{L^5})](NO_3)\cdot 3H_2O$. View down to *y* axis. Carbon-bound hydrogen atoms are not shown. Colour code: Cu: green, Li: orange, P: yellow, O: red, N: blue, C: black, H: white.

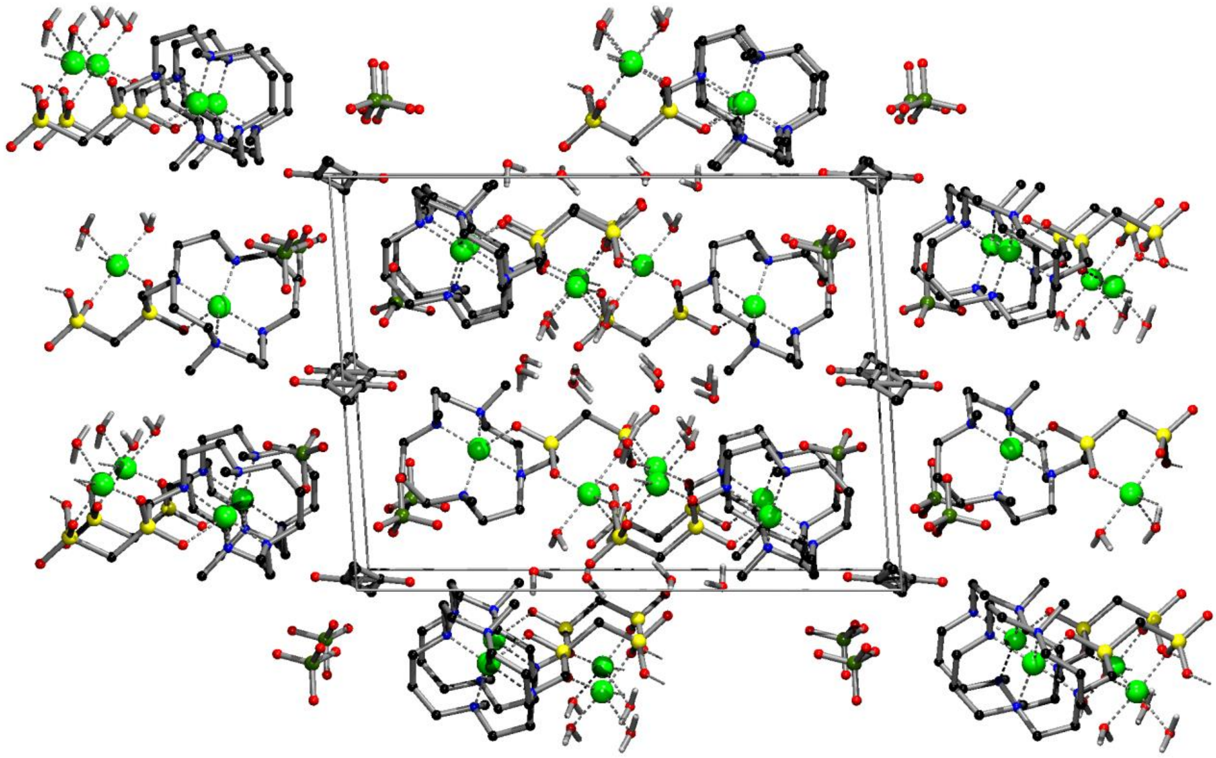

Figure S3. Crystal packing found in crystal structure of {$Cu(H_2O)_2[Cu(\mathbf{L^7})]$}($ClO_4$)·$2H_2O$·0.5acetone. View down to *y* axis. Carbon-bound hydrogen atoms are not shown. Colour code: Cu: green, P: yellow, O: red, N: blue, C: black, H: white.

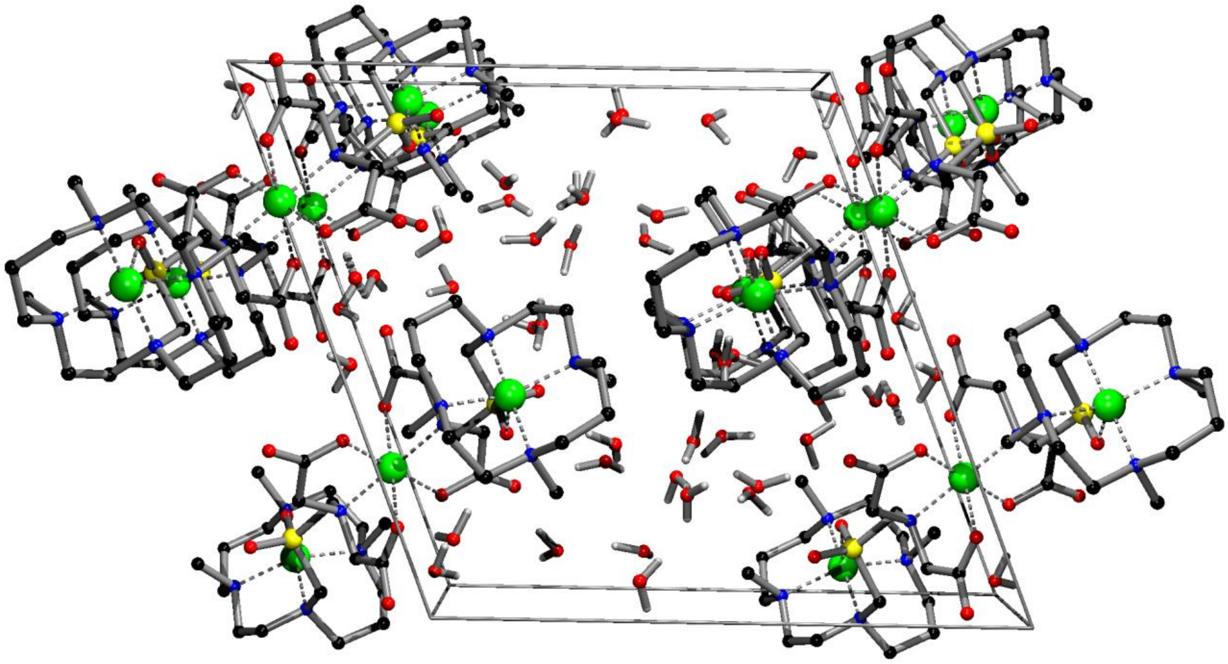

Figure S4. Crystal packing found in crystal structure of {$Cu[Cu(\mathbf{L^{10}})]_2$}·$19H_2O$. View down to *y* axis. Carbon-bound hydrogen atoms are not shown. Colour code: Cu: green, P: yellow, O: red, N: blue, C: black, H: white.

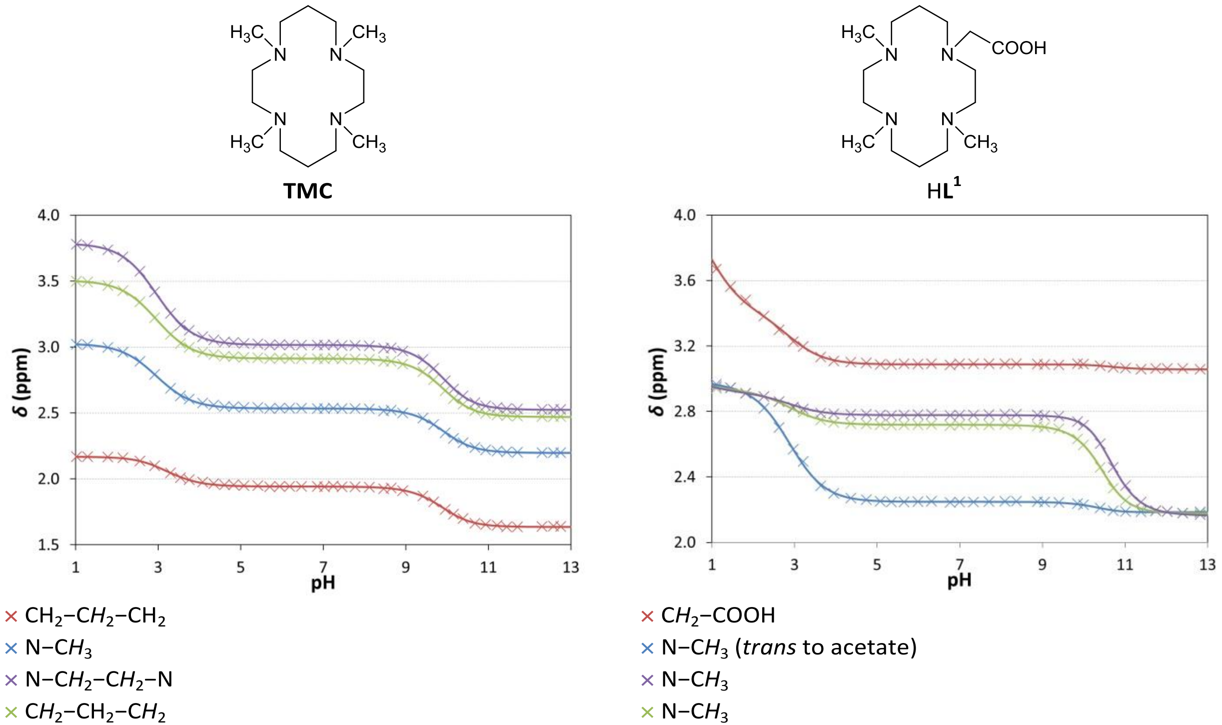

Figure S5. ^{1}H NMR titration data used for determination of protonation constants and protonation sites of **TMC** and H**L**^{1}. Lines show the best fits using protonation constants from Table 2.

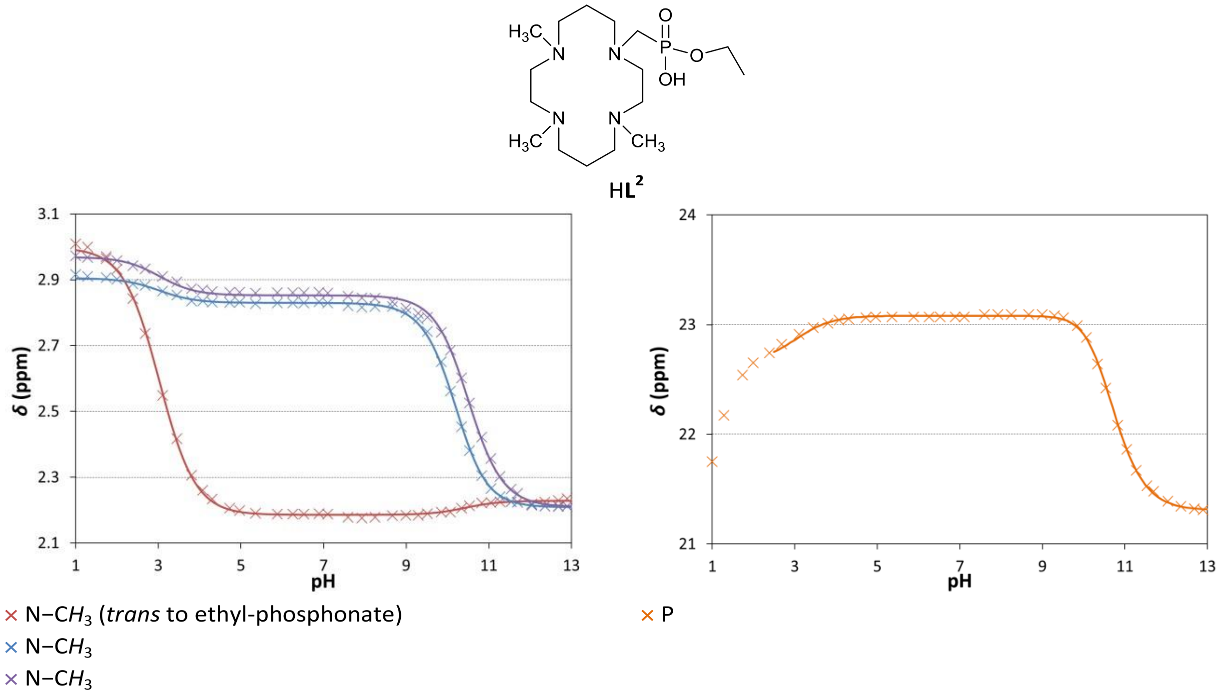

Figure S6. ^{1}H and ^{31}P NMR titration data used for determination of protonation constants and protonation sites of H**L**^{2}. Lines show the best fits using protonation constants from Table 2.

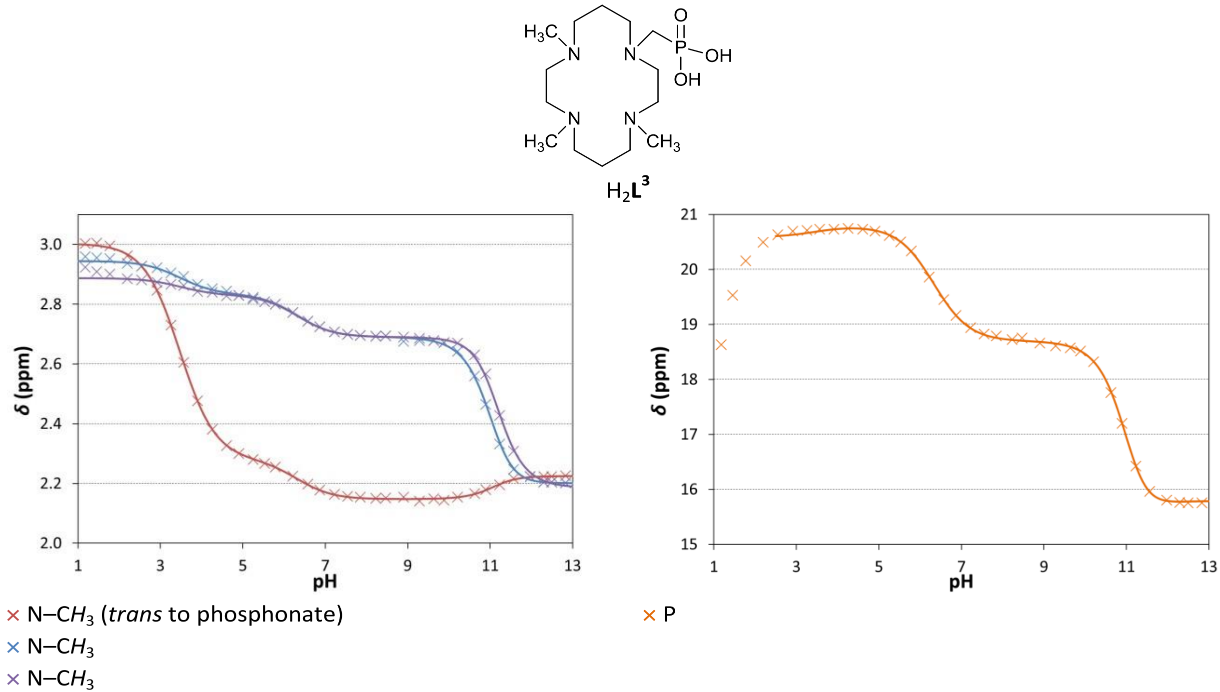

Figure S7. ^{1}H and ^{31}P NMR titration data used for determination of protonation constants and protonation sites of H_2**L**^{3}. Lines show the best fits using protonation constants from Table 2.

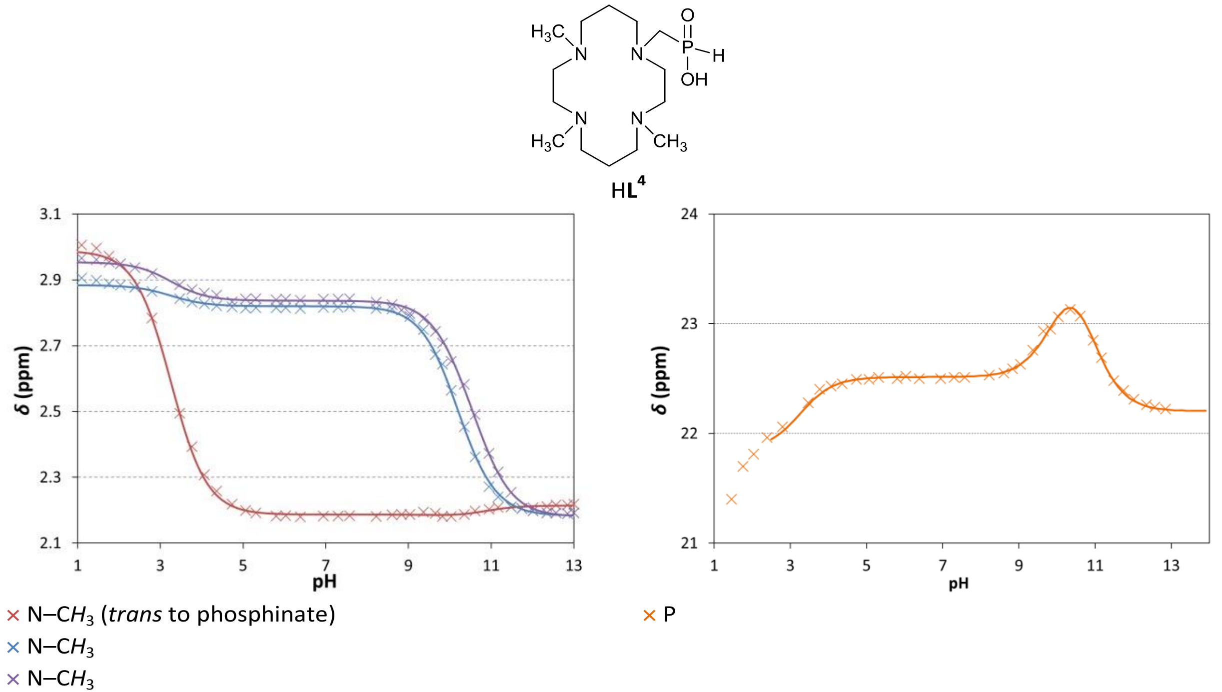

Figure S8. ^{1}H and ^{31}P NMR titration data used for determination of protonation constants and protonation sites of H**L**^{4}. Lines show the best fits using protonation constants from Table 2.

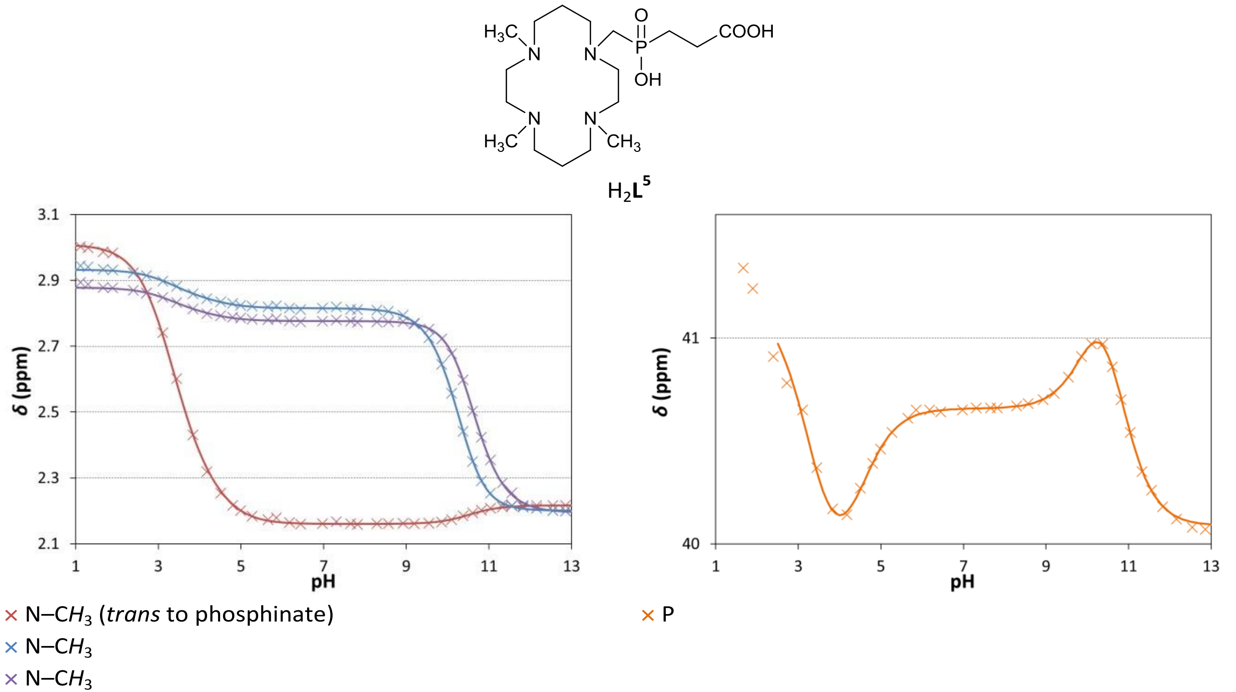

Figure S9. ^{1}H and ^{31}P NMR titration data used for determination of protonation constants and protonation sites of $H_2\mathbf{L}^5$. Lines show the best fits using protonation constants from Table 2.

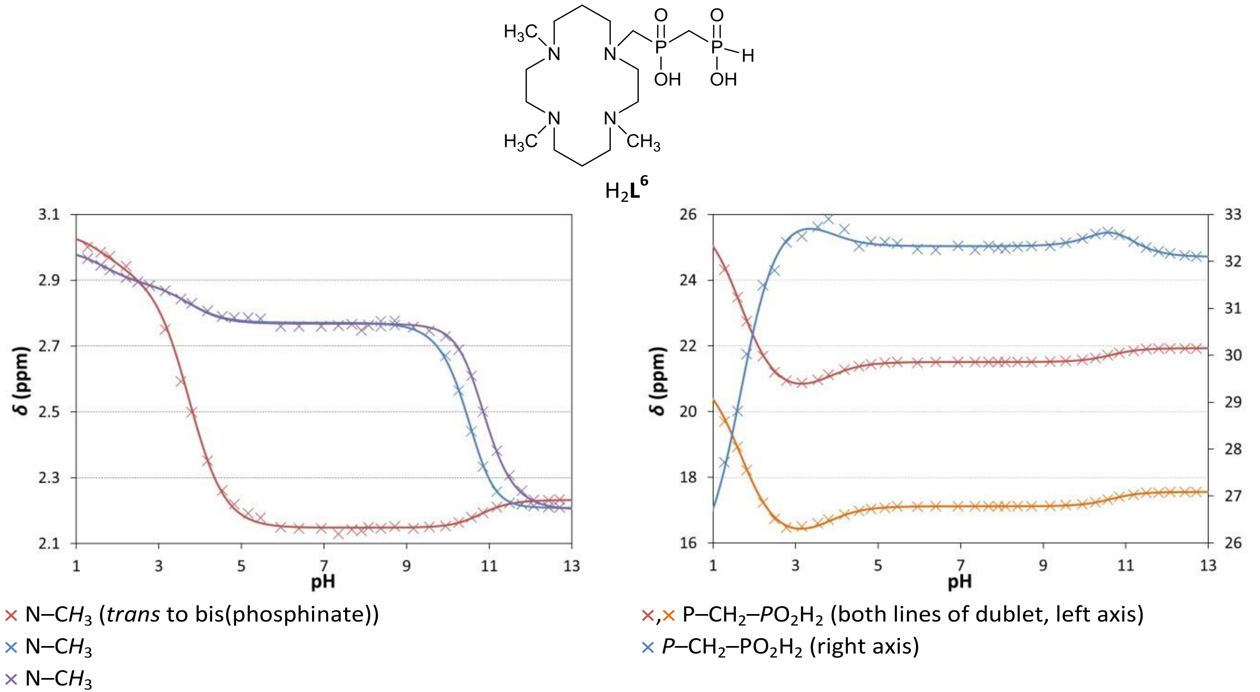

Figure S10. ^{1}H and ^{31}P NMR titration data used for determination of protonation constants and protonation sites of $H_2\mathbf{L}^6$. Lines show the best fits using protonation constants from Table 2.

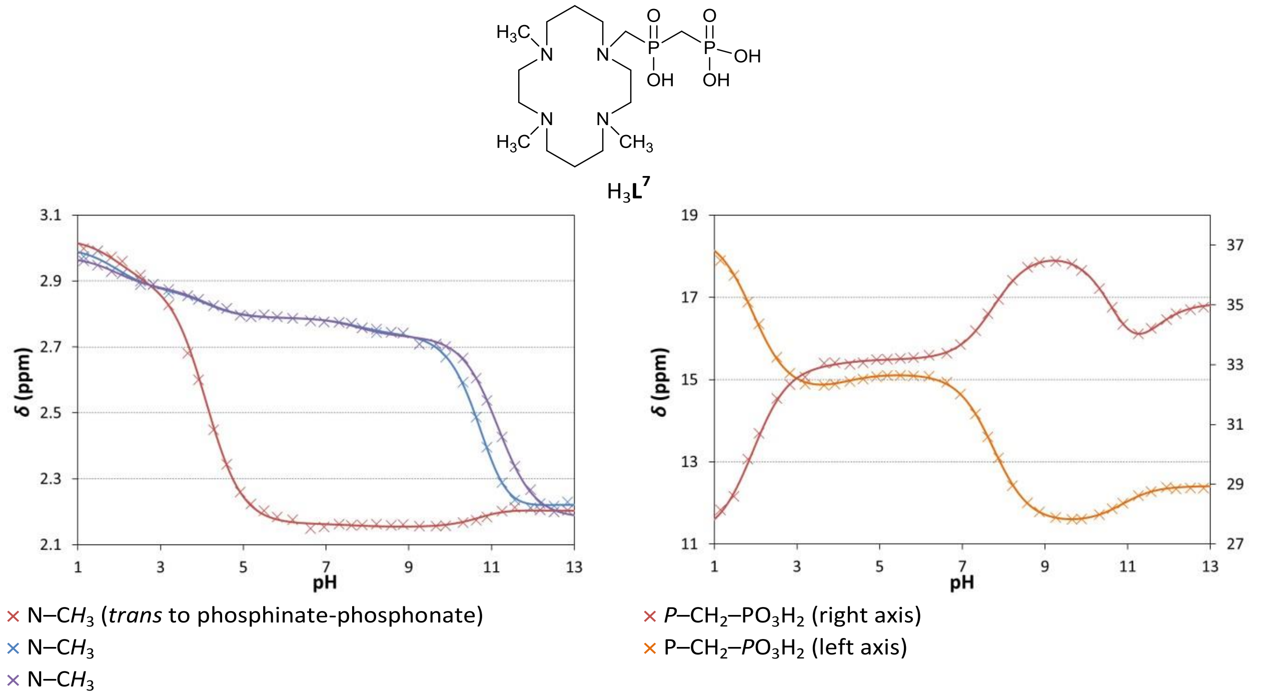

Figure S11. ^{1}H and ^{31}P NMR titration data used for determination of protonation constants and protonation sites of H_3**L**^{7}. Lines show the best fits using protonation constants from Table 2.

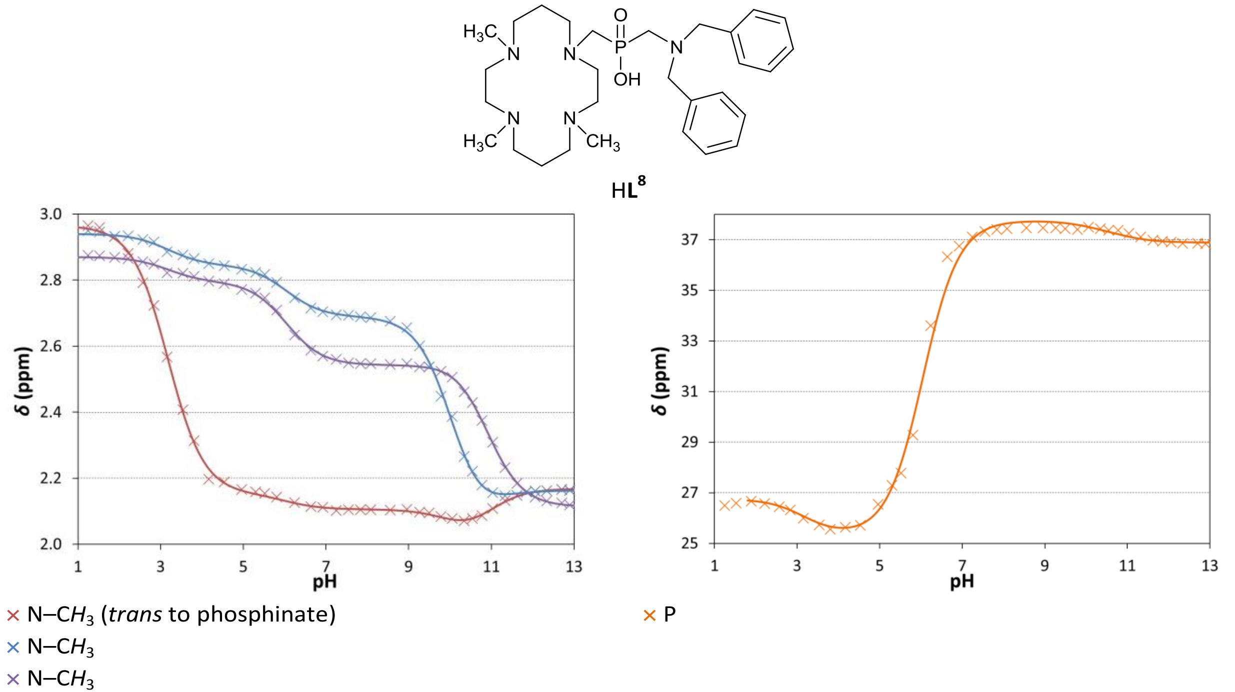

Figure S12. ^{1}H and ^{31}P NMR titration data used for determination of protonation constants and protonation sites of H**L**^{8}. Lines show the best fits using protonation constants from Table 2.

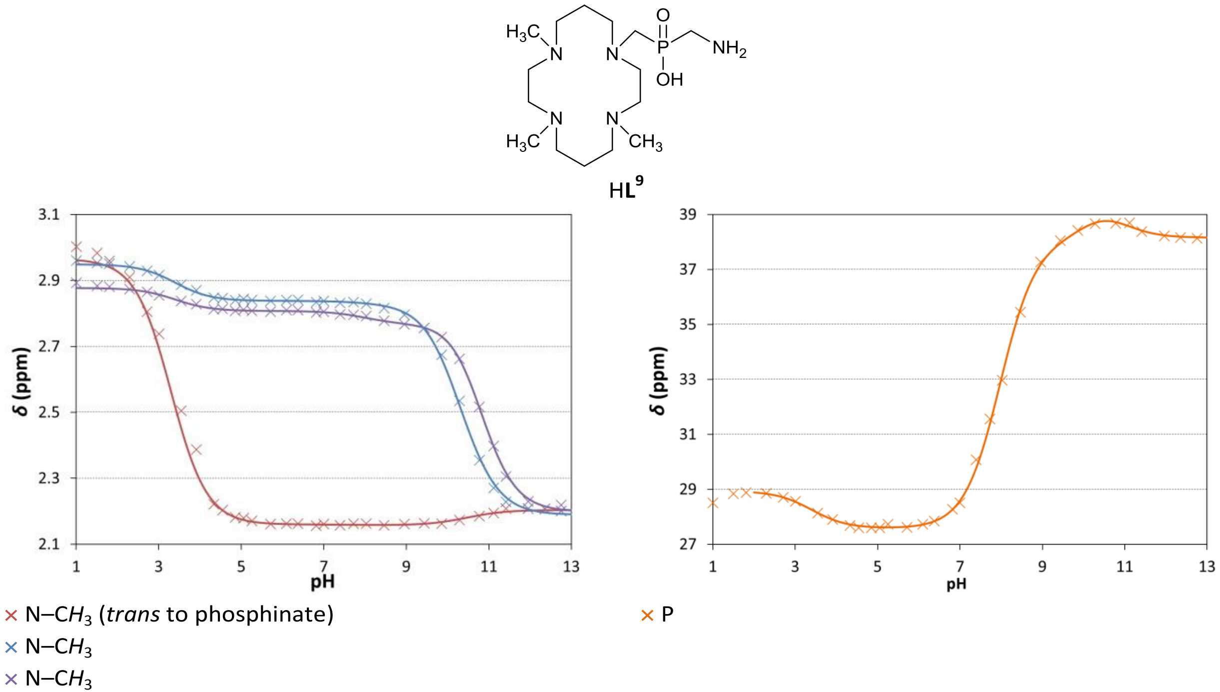

Figure S13. ^{1}H and ^{31}P NMR titration data used for determination of protonation constants and protonation sites of H**L**^{9}. Lines show the best fits using protonation constants from Table 2.

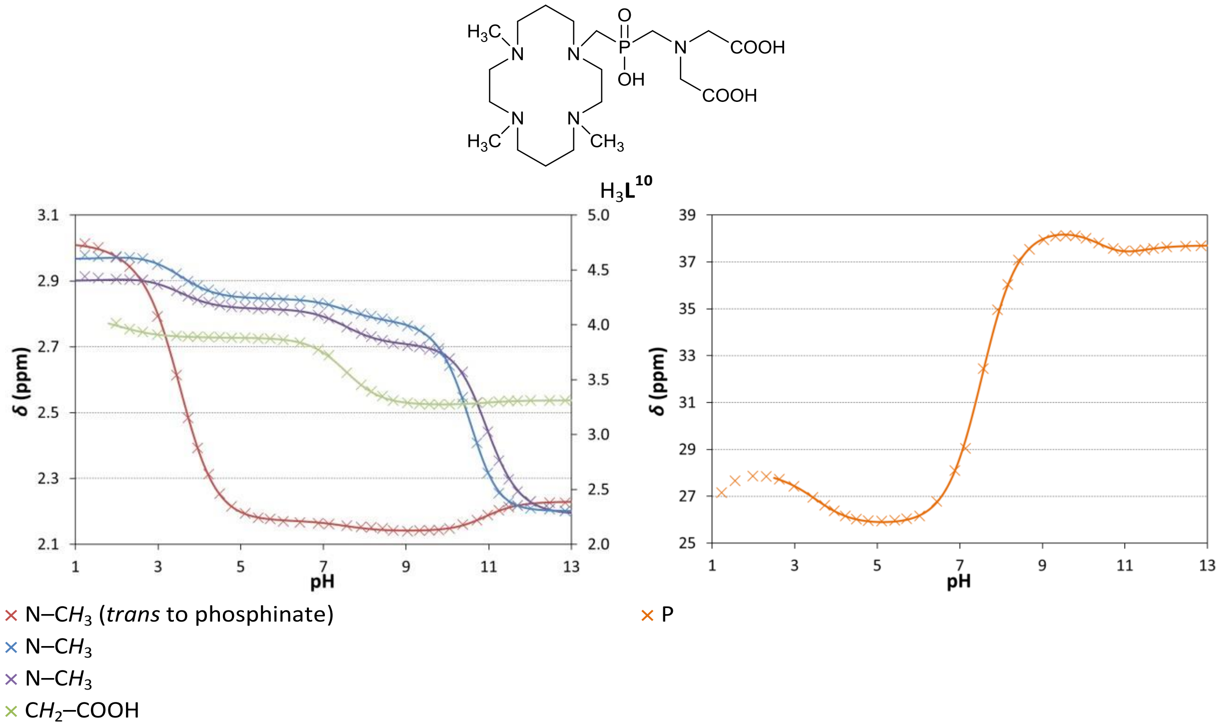

Figure S14. ^{1}H and ^{31}P NMR titration data used for determination of protonation constants and protonation sites of H$_3$**L**^{10}. Lines show the best fits using protonation constants from Table 2.

Table S1. Overall protonation constants (logβ_h)^a of the studied ligands obtained by ^{1}H and ^{31}P NMR titrations.^{b}

	h				
	1	2	3	4	5
TMC	9.80(12)	19.17(9)	22.46(12)	25.14(15)	–
H**L**^{1}	10.60(2)	21.08(3)	23.96(7)	24.81(12)	–
H**L**^{2}	10.67(1)	20.81(2)	23.83(2)	–	–
H_2**L**^{3}	11.11(4)	22.26(4)	28.59(4)	32.06(4)	–
H**L**^{4}	10.82(1)	20.85(2)	24.11(2)	–	–
H_2**L**^{5}	10.63(2)	20.89(2)	25.32(4)	28.61(3)	–
H_2**L**^{6}	10.85(7)	21.42(8)	25.15(9)	26.83(8)	–
H_3**L**^{7}	11.38(4)	22.13(2)	29.89(2)	33.99(3)	35.93(3)
H**L**^{8}	10.95(2)	20.97(2)	27.01(3)	30.19(3)	–
H**L**^{9}	10.87(6)	20.99(8)	28.96(8)	32.36(8)	–
H_3**L**^{10}	11.03(6)	21.57(6)	29.11(6)	32.66(7)	34.73(4)

^{a} $\beta_h = [H_hL]/\{[H]^h\cdot[L]\}$; charges are omitted. ^{b} Conditions used: 25 °C, 0.1 M KCl.

Table S2. Dependence of the pseudo-first-order formation rate constant $^{f}k_{obs}$ [s^{-1}] on Cu(II) concentration.^{a}

c(Cu) [mM]	Cu(II) excess	**TMC**	H**L**^{1}	H**L**^{2}	H_2**L**^{3}	H**L**^{4}	H_2**L**^{5}
5	50×	$8.639(5)\cdot10^{-4}$	5.658(2)	$7.20(1)\cdot10^{-3}$	$1.513(1)\cdot10^{-2}$	$1.520(4)\cdot10^{-2}$	$1.047(1)\cdot10^{-2}$
4	40×	$7.361(2)\cdot10^{-4}$	4.612(3)	$5.492(4)\cdot10^{-3}$	$1.231(8)\cdot10^{-2}$	$1.140(2)\cdot10^{-2}$	$8.52(1)\cdot10^{-3}$
3	30×	$5.458(2)\cdot10^{-4}$	3.374(4)	$4.198(3)\cdot10^{-3}$	$9.215(4)\cdot10^{-3}$	$8.79(1)\cdot10^{-3}$	$6.46(1)\cdot10^{-3}$
2	20×	$3.521(1)\cdot10^{-4}$	2.223(1)	$2.777(2)\cdot10^{-3}$	$6.552(5)\cdot10^{-3}$	$5.711(7)\cdot10^{-3}$	$4.275(5)\cdot10^{-3}$
1	10×	$1.901(1)\cdot10^{-4}$	1.065(1)	$1.382(1)\cdot10^{-3}$	$3.229(3)\cdot10^{-3}$	$2.714(3)\cdot10^{-3}$	$1.932(2)\cdot10^{-3}$
0.5	5×	–	$5.797(2)\cdot10^{-1}$	–	–		
0.4	4×	–	$4.614(1)\cdot10^{-1}$	–	–		
0.3	3×	–	$3.385(2)\cdot10^{-1}$	–	–		
0.2	2×	–	$2.28(1)\cdot10^{-1}$	–	–		
0.1	1×	–	$1.900(3)\cdot10^{-1}$	–	–		

c(Cu) [mM]	Cu(II) excess	H_2**L**^{6}	H_3**L**^{7}	H**L**^{8}	H**L**^{9}	H_3**L**^{10}
5	50×	$1.002(3)\cdot10^{-1}$	$1.72(1)\cdot10^{-1}$	$5.385(3)\cdot10^{-3}$	$6.82(6)\cdot10^{-3}$	$3.045(2)\cdot10^{-3}$
4	40×	$8.21(3)\cdot10^{-2}$	$1.53(1)\cdot10^{-1}$	$4.279(2)\cdot10^{-3}$	$5.555(3)\cdot10^{-3}$	$2.544(2)\cdot10^{-3}$
3	30×	$6.74(5)\cdot10^{-2}$	$1.21(3)\cdot10^{-1}$	$3.261(2)\cdot10^{-3}$	$4.141(2)\cdot10^{-3}$	$1.950(1)\cdot10^{-3}$
2	20×	$4.39(1)\cdot10^{-2}$	$6.7(1)\cdot10^{-2}$	$2.288(1)\cdot10^{-3}$	$2.821(1)\cdot10^{-3}$	$1.308(1)\cdot10^{-3}$
1	10×	$2.37(4)\cdot10^{-2}$	$4.26(1)\cdot10^{-2}$	$1.153(1)\cdot10^{-3}$	$1.392(1)\cdot10^{-3}$	$6.260(4)\cdot10^{-4}$

^{a} Conditions used: pH = 3.00, t = 25 °C, I = 0.1 M KCl, c(ligand) = 0.1 mM, 10–50× excess of Cu(II).

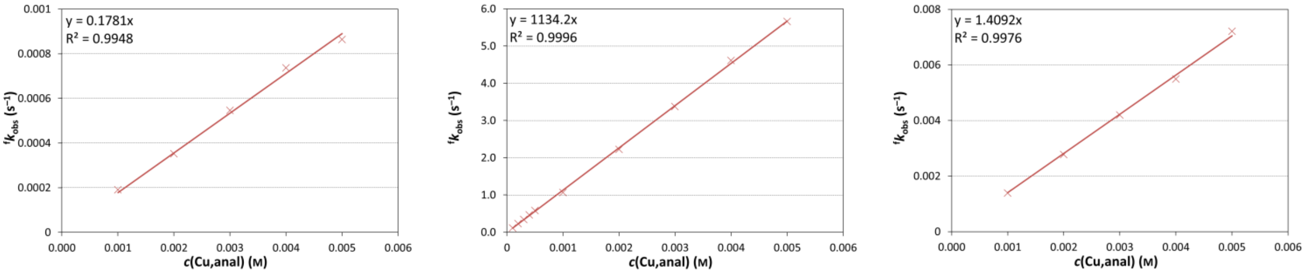

Cu–**TMC** Cu–H$\mathbf{L}^{1}$ Cu–H$\mathbf{L}^{2}$

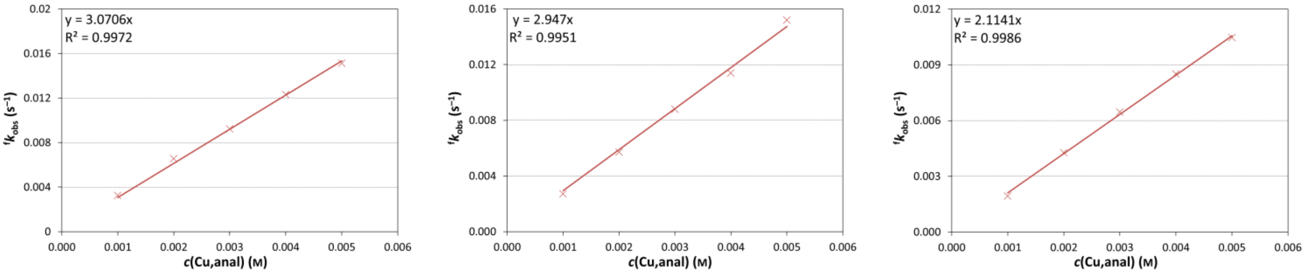

Cu–$H_2\mathbf{L}^{3}$ Cu–H$\mathbf{L}^{4}$ Cu–$H_2\mathbf{L}^{5}$

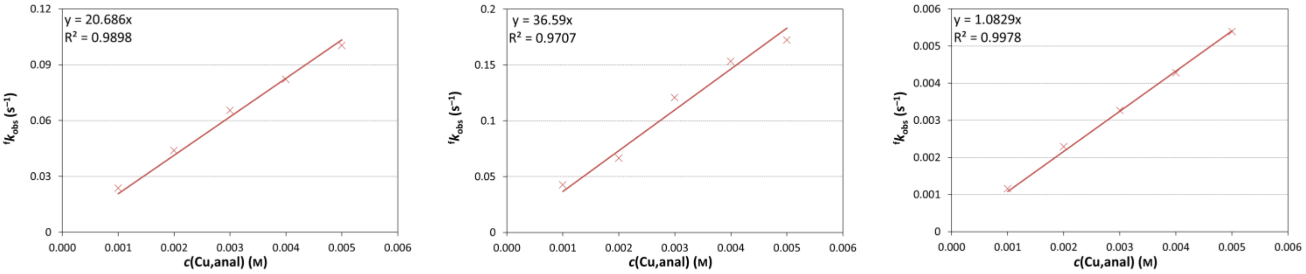

Cu–$H_2\mathbf{L}^{6}$ Cu–$H_3\mathbf{L}^{7}$ Cu–H$\mathbf{L}^{8}$

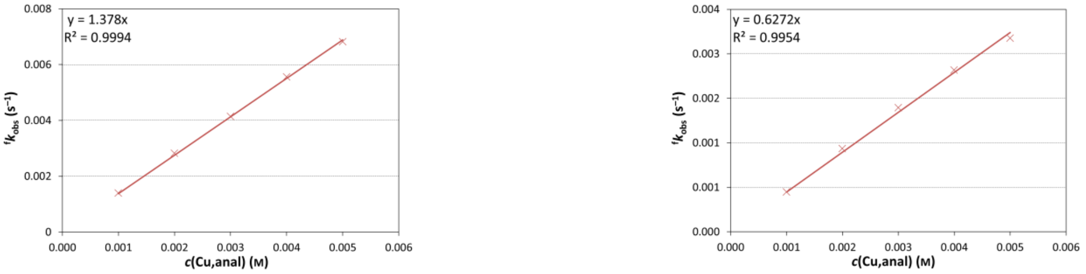

Cu–H$\mathbf{L}^{9}$ Cu–$H_3\mathbf{L}^{10}$

Figure S15. Dependence of the pseudo-first-order formation rate constant $^{f}k_{obs}$ on Cu(II) concentration [pH = 3.00, *t* = 25 °C, *I* = 0.1 м KCl, *c*(ligand) = 0.1 mм, 10–50× excess of Cu(II)].

Table S3. Dependence of the pseudo-first-order formation rate constant ${}^{f}k_{obs}$ [s^{-1}] on ligand concentration.[a]

c(L) [μM]	ligand excess	**TMC**	H**L**^{1}	H**L**^{2}	H$_2$**L**^{3}	H**L**^{4}	H$_2$**L**^{5}
250	50×	$5.21(2)\cdot10^{-5}$	$3.31(1)\cdot10^{-1}$	$3.91(1)\cdot10^{-4}$	$7.64(2)\cdot10^{-4}$	$8.66(3)\cdot10^{-4}$	$6.10(1)\cdot10^{-4}$
200	40×	$3.88(2)\cdot10^{-5}$	$2.49(1)\cdot10^{-1}$	$3.44(1)\cdot10^{-4}$	$5.77(1)\cdot10^{-4}$	$6.52(2)\cdot10^{-4}$	$4.82(1)\cdot10^{-4}$
150	30×	$3.32(2)\cdot10^{-5}$	$1.880(5)\cdot10^{-1}$	$2.26(1)\cdot10^{-4}$	$3.98(1)\cdot10^{-4}$	$4.00(1)\cdot10^{-4}$	$3.53(1)\cdot10^{-4}$
100	20×	$2.14(2)\cdot10^{-5}$	$1.223(4)\cdot10^{-1}$	$1.394(2)\cdot10^{-4}$	$2.73(1)\cdot10^{-4}$	$3.03(1)\cdot10^{-4}$	$2.25(1)\cdot10^{-4}$
50	10×	$9.6(3)10^{-6}$	$5.22(3)\cdot10^{-2}$	$6.560(3)\cdot10^{-5}$	$1.95(1)\cdot10^{-4}$	$1.62(1)\cdot10^{-4}$	$1.22(1)\cdot10^{-4}$

c(L) [μM]	ligand excess	H$_2$**L**^{6}	H$_3$**L**^{7}	H**L**^{8}	H**L**^{9}	H$_3$**L**^{10}
250	50×	$5.86(2)\cdot10^{-3}$	$1.24(1)\cdot10^{-2}$	$2.383(3)\cdot10^{-4}$	$2.94(2)\cdot10^{-4}$	$4.45(1)\cdot10^{-5}$
200	40×	$4.99(2)\cdot10^{-3}$	$9.38(6)\cdot10^{-3}$	$1.88(1)\cdot10^{-4}$	$2.31(1)\cdot10^{-4}$	$4.42(1)\cdot10^{-5}$
150	30×	$3.73(1)\cdot10^{-3}$	$6.46(3)\cdot10^{-3}$	$1.359(4)\cdot10^{-4}$	$1.751(4)\cdot10^{-4}$	$3.34(1)\cdot10^{-5}$
100	20×	$2.46(1)\cdot10^{-3}$	$4.61(2)\cdot10^{-3}$	$8.49(2)\cdot10^{-5}$	$1.300(3)\cdot10^{-4}$	$2.46(1)\cdot10^{-5}$
50	10×	$1.100(2)\cdot10^{-3}$	$2.05(1)\cdot10^{-3}$	$4.24(4)\cdot10^{-5}$	$7.47(1)\cdot10^{-5}$	$2.70(1)\cdot10^{-5}$

[a] Conditions used: pH = 3.00, t = 25 °C, I = 0.1 M KCl, c[Cu(II)] = 5 μM, 10–50× excess of ligand.

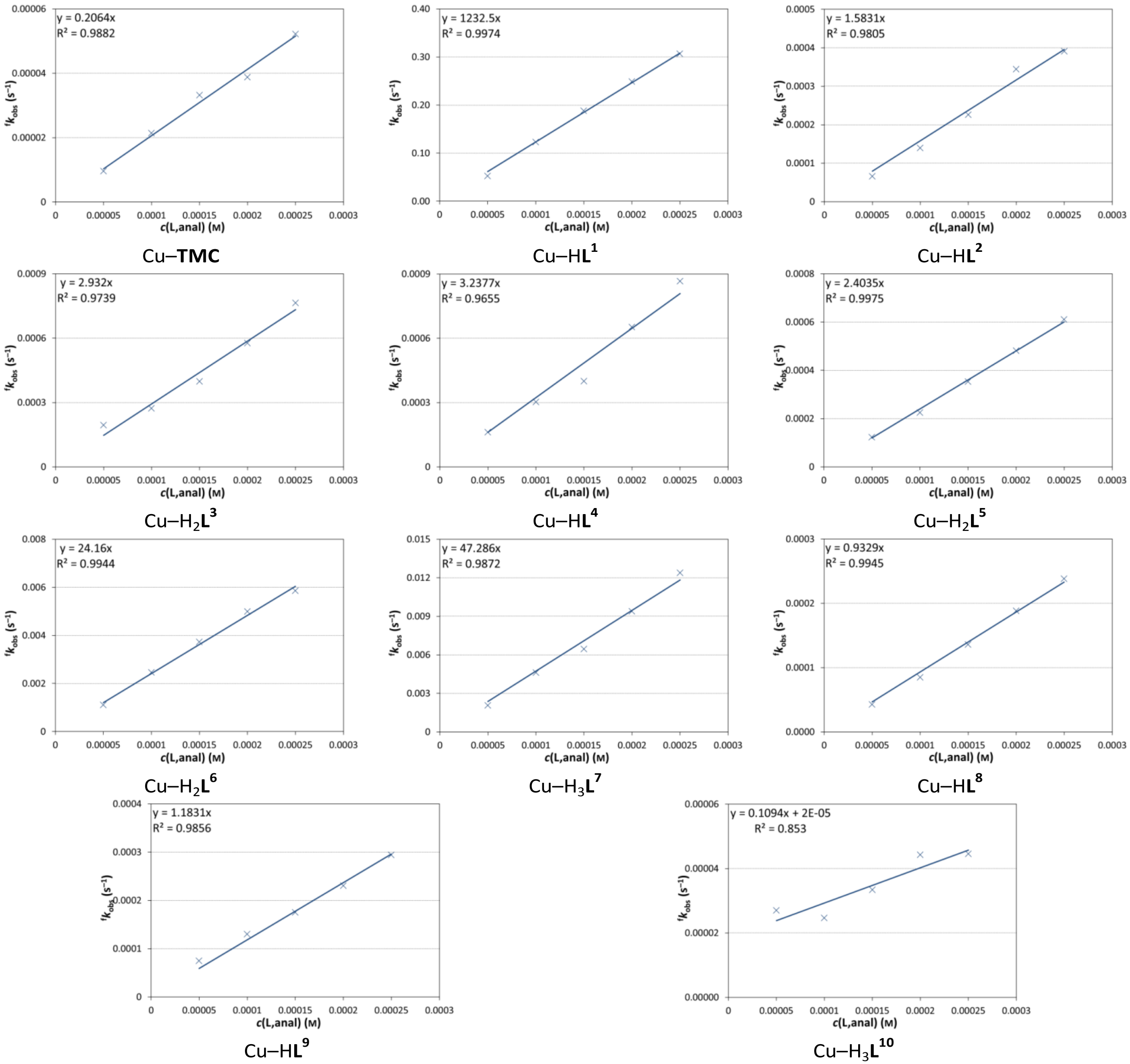

Cu–**TMC** Cu–H**L**^{1} Cu–H**L**^{2}

Cu–H$_2$**L**^{3} Cu–H**L**^{4} Cu–H$_2$**L**^{5}

Cu–H$_2$**L**^{6} Cu–H$_3$**L**^{7} Cu–H**L**^{8}

Cu–H**L**^{9} Cu–H$_3$**L**^{10}

Figure S16. Dependence of the pseudo-first-order formation rate constant ${}^{f}k_{obs}$ on ligand concentration {pH = 3.00, I = 0.1 M KCl, t = 25 °C, c[Cu(II)] = 5 μM, 10–50× excess of ligand}.

Table S4. The second-order rate constants ${}^{f}k_2$ of Cu(II) complex formation obtained at different pH.[a]

Cu–**TMC**		Cu–H**L**^{1}		Cu–H$_2$**L**^{3}		Cu–H$_2$**L**^{6}		Cu–H$_3$**L**^{7}	
pH	${}^{f}k_2$ [s^{-1}]	pH	${}^{f}k_2$ [s^{-1}·mol^{-1}·dm^3]	pH	${}^{f}k_2$ [s^{-1}·mol^{-1}·dm^3]	pH	${}^{f}k_2$ [s^{-1}·mol^{-1}·dm^3]	pH	${}^{f}k_2$ [s^{-1}·mol^{-1}·dm^3]
2.81	$3.10(1)\cdot10^{-1}$	2.44	$6.03(1)\cdot10^{+2}$	2.59	3.010(5)	2.64	$2.455(4)\cdot10^{+1}$	2.71	$5.57(1)\cdot10^{+1}$
3.00	$3.306(2)\cdot10^{-1}$	2.82	$8.92(2)\cdot10^{+2}$	2.98	5.15(1)	3.03	$4.070(5)\cdot10^{+1}$	3.01	$9.19(1)\cdot10^{+1}$
3.21	$5.000(3)\cdot10^{-1}$	3.00	$1.060(2)\cdot10^{+2}$	3.19	7.85(1)	3.21	$5.653(9)\cdot10^{+1}$	3.24	$1.421(3)\cdot10^{+2}$
3.51	$7.90(1)\cdot10^{-1}$	3.31	$1.30(3)\cdot10^{+3}$	3.50	$1.500(4)\cdot10^{+1}$	3.49	$8.67(1)\cdot10^{+1}$	3.55	$2.63(1)\cdot10^{+2}$
3.84	1.518(3)	3.70	$1.61(3)\cdot10^{+3}$	3.90	$3.84(2)\cdot10^{+1}$	3.82	$1.351(3)\cdot10^{+2}$	3.94	$5.82(2)\cdot10^{+2}$
4.13	2.41(1)	4.02	$1.90(4)\cdot10^{+3}$	4.24	$8.1(1)\cdot10^{+1}$	4.10	$1.99(1)\cdot10^{+2}$	4.32	$1.010(2)\cdot10^{+3}$
4.28	3.245(4)	4.21	$3.01(6)\cdot10^{+3}$	4.26	$1.159(3)\cdot10^{+2}$	4.26	$2.573(3)\cdot10^{+2}$	4.28	$1.056(2)\cdot10^{+3}$
4.49	5.37(1)	4.64	$4.41(1)\cdot10^{+3}$	4.45	$2.23(1)\cdot10^{+2}$	4.45	$3.596(4)\cdot10^{+2}$	4.49	$1.523(2)\cdot10^{+3}$
4.83	$1.167(1)\cdot10^{+1}$	4.92	$5.15(1)\cdot10^{+3}$	4.80	$6.07(2)\cdot10^{+2}$	4.78	$6.37(1)\cdot10^{+2}$	4,83	$2.970(4)\cdot10^{+3}$
5.09	$1.898(2)\cdot10^{+1}$	5.24	$5.96(1)\cdot10^{+3}$	5.06	$1.427(4)\cdot10^{+3}$	5.05	$1.011(2)\cdot10^{+3}$	5.10	$4.94(1)\cdot10^{+3}$
5.37	$3.49(1)\cdot10^{+1}$	5.48	$5.19(1)\cdot10^{+3}$	5.33	$3.46(1)\cdot10^{+3}$	5.31	$1.679(3)\cdot10^{+3}$	5.39	$8.80(2)\cdot10^{+3}$
5.68	$5.2(1)\cdot10^{+1}$	5.84	$7.14(2)\cdot10^{+3}$	5.57	$6.40(4)\cdot10^{+3}$	5.60	$3.975(3)\cdot10^{+3}$	5.60	$1.291(2)\cdot10^{+4}$
5.84	$8.32(1)\cdot10^{+1}$	6.14	$8.99(2)\cdot10^{+3}$	5.80	$2.097(5)\cdot10^{+4}$	5.80	$6.67(1)\cdot10^{+3}$	5.83	$2.710(2)\cdot10^{+4}$
6.05	$1.257(2)\cdot10^{+2}$	6.60	$1.280(3)\cdot10^{+4}$	5.99	$3.97(1)\cdot10^{+4}$	6.01	$1.001(1)\cdot10^{+4}$	6.02	$4.0(1)\cdot10^{+4}$
6.20	$2.05(4)\cdot10^{+2}$	6.83	$1.679(2)\cdot10^{+4}$	6.28	$8.09(2)\cdot10^{+4}$	6.30	$1.687(2)\cdot10^{+4}$	6.31	$7.05(1)\cdot10^{+4}$
6.69	$5.5(5)\cdot10^{+2}$			6.48	$1.423(5)\cdot10^{+5}$	6.51	$2.583(3)\cdot10^{+5}$	6.51	$1.255(3)\cdot10^{+5}$
6.90	$7.5(1)\cdot10^{+2}$			6.76	$1.85(1)\cdot10^{+5}$	6.76	$3.305(8)\cdot10^{+5}$	6.81	$1.83(1)\cdot10^{+5}$

[a] Conditions used: *t* = 25 °C, *I* = 0.1 M KCl, *c*(ligand) = 0.1 mM, 10× excess of Cu(II).

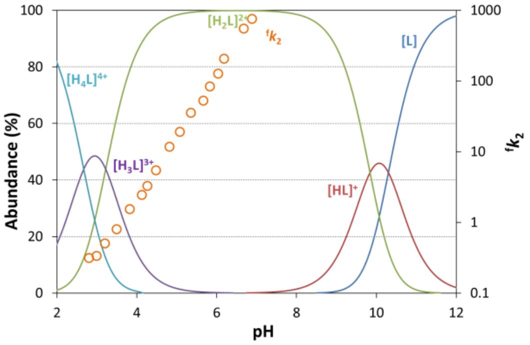

TMC

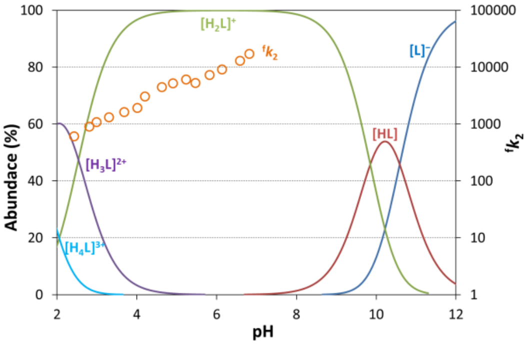

HL^1

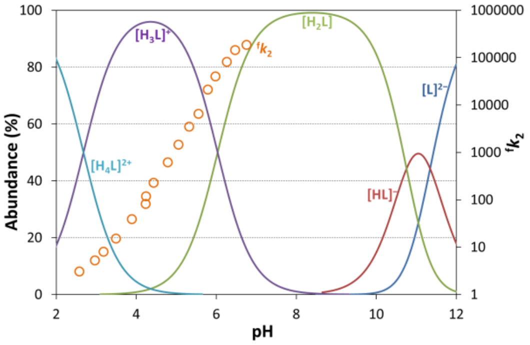

H_2L^3

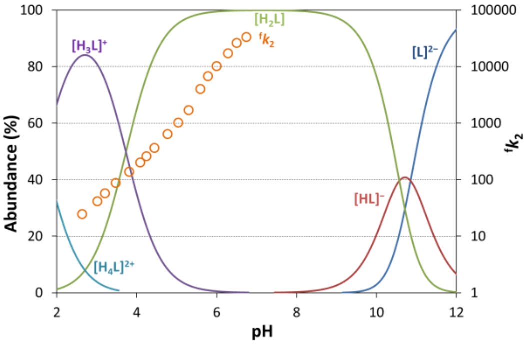

H_2L^6

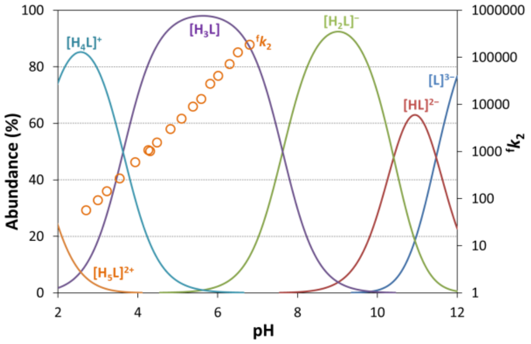

H_3L^7

Figure S17. Overlay of the observed second-order rate constants ${}^{f}k_2$ of Cu(II) complex formation with appropriate ligand distribution diagrams.

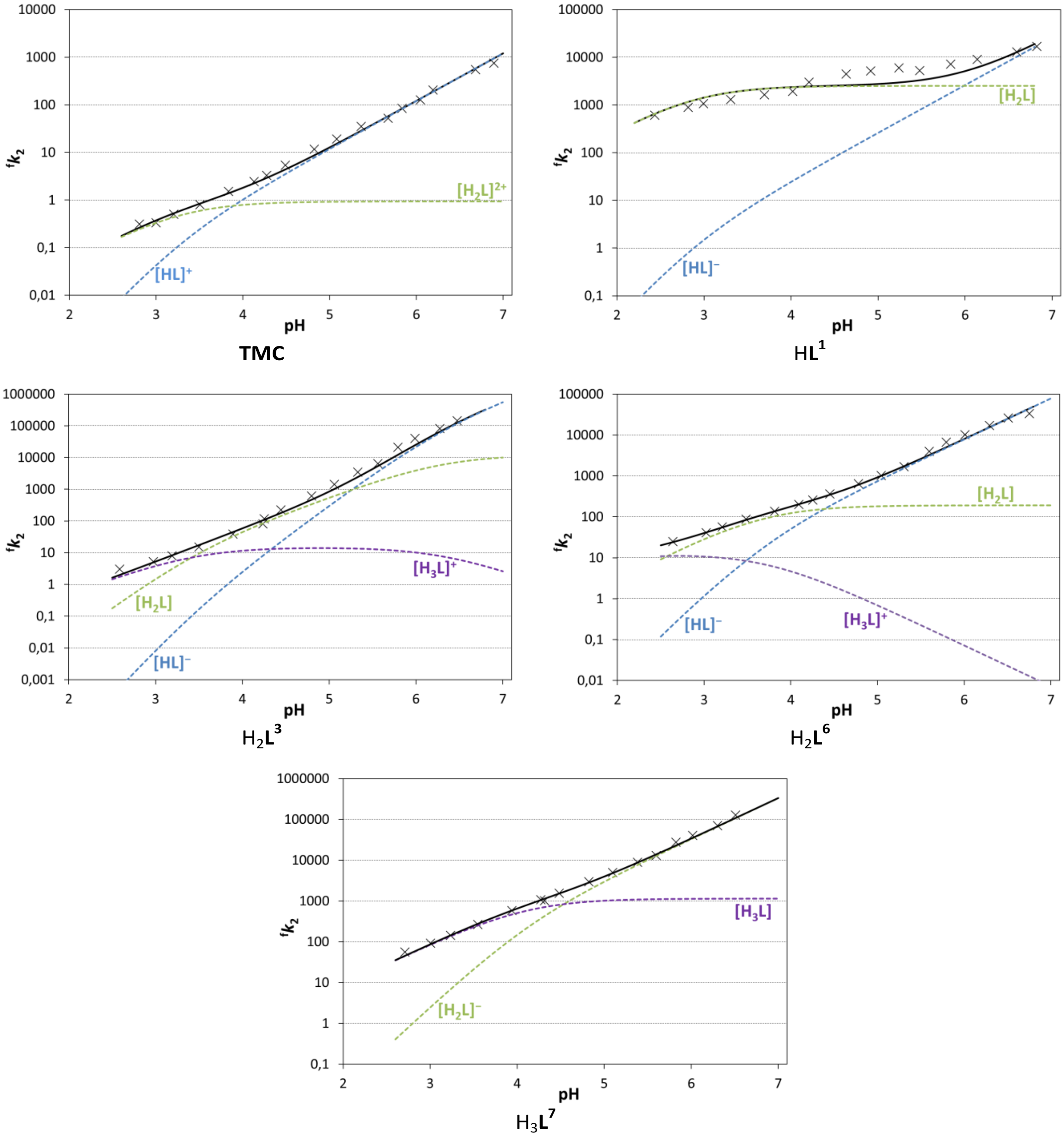

Figure S18. pH dependence of contributions of reactivity of differently protonated ligand species to the overall second-order rate constants ${}^{f}k_2$ of Cu(II) complex formation.

Table S5. The observed first-order rate constants ${}^{\mathrm{d}}k_{\mathrm{obs}}$ [s^{-1}] for acid-assisted dissociation of Cu(II) complexes at different acid concentrations and temperatures.[a]

		Cu–**TMC**		
[H$^+$]	25 °C	35 °C	45 °C	55 °C
4.89	$4.44(4)\cdot10^{-2}$	$1.23(1)\cdot10^{-1}$	$2.63(6)\cdot10^{-1}$	$5.70(2)\cdot10^{-1}$
4.00	$4.25(2)\cdot10^{-2}$	$1.12(1)\cdot10^{-1}$	$2.43(6)\cdot10^{-1}$	$5.15(2)\cdot10^{-1}$
3.00	$4.00(2)\cdot10^{-2}$	$9.92(1)\cdot10^{-2}$	$2.12(3)\cdot10^{-1}$	$4.31(1)\cdot10^{-1}$
2.00	$3.78(2)\cdot10^{-2}$	$9.04(1)\cdot10^{-2}$	$1.79(2)\cdot10^{-1}$	$3.77(1)\cdot10^{-1}$
1.00	$3.19(2)\cdot10^{-2}$	$6.42(4)\cdot10^{-2}$	$1.32(1)\cdot10^{-1}$	$2.58(1)\cdot10^{-1}$
0.50	$2.17(1)\cdot10^{-2}$	$4.16(2)\cdot10^{-2}$	$8.16(5)\cdot10^{-2}$	$1.54(2)\cdot10^{-1}$
0.10	$5.03(1)\cdot10^{-3}$	$8.61(1)\cdot10^{-3}$	$1.61(5)\cdot10^{-2}$	$2.77(1)\cdot10^{-2}$
0.05	$2.64(1)\cdot10^{-3}$	$4.73(1)\cdot10^{-3}$	$6.62(1)\cdot10^{-3}$	$1.06(1)\cdot10^{-2}$
		Cu–H**L**$^{\mathbf{1}}$		
[H$^+$]	25 °C	35 °C	45 °C	55 °C
4.89	$1.44(3)\cdot10^{-3}$	$2.74(5)\cdot10^{-3}$	$6.15(3)\cdot10^{-3}$	$1.19(4)\cdot10^{-2}$
4.00	$1.43(3)\cdot10^{-3}$	$2.93(6)\cdot10^{-3}$	$6.19(2)\cdot10^{-3}$	$1.23(5)\cdot10^{-2}$
3.00	$1.30(3)\cdot10^{-3}$	$3.13(6)\cdot10^{-3}$	$6.30(4)\cdot10^{-3}$	$1.22(6)\cdot10^{-2}$
2.00	$1.35(2)\cdot10^{-3}$	$3.24(6)\cdot10^{-3}$	$6.37(3)\cdot10^{-3}$	$1.21(5)\cdot10^{-2}$
1.00	$1.30(2)\cdot10^{-3}$	$3.06(6)\cdot10^{-3}$	$6.15(2)\cdot10^{-3}$	$1.21(5)\cdot10^{-2}$
0.50	$1.20(2)\cdot10^{-3}$	$2.87(6)\cdot10^{-3}$	$5.27(2)\cdot10^{-3}$	$1.02(5)\cdot10^{-2}$
0.10	$8.05(1)\cdot10^{-4}$	$1.97(4)\cdot10^{-3}$	$3.79(1)\cdot10^{-3}$	$7.02(2)\cdot10^{-3}$
0.05	$5.88(1)\cdot10^{-4}$	$1.53(3)\cdot10^{-3}$	$2.88(5)\cdot10^{-3}$	$5.48(2)\cdot10^{-3}$
		Cu–H$_2$**L**$^{\mathbf{3}}$		
[H$^+$]	25 °C	35 °C	45 °C	55 °C
4.89	$6.40(3)\cdot10^{-4}$	$1.89(3)\cdot10^{-3}$	$4.57(7)\cdot10^{-3}$	$1.43(8)\cdot10^{-2}$
4.00	$6.04(1)\cdot10^{-4}$	$1.89(3)\cdot10^{-3}$	$4.33(8)\cdot10^{-3}$	$1.28(10)\cdot10^{-2}$
3.00	$4.67(5)\cdot10^{-4}$	$1.94(2)\cdot10^{-3}$	$4.36(8)\cdot10^{-3}$	$1.22(11)\cdot10^{-2}$
2.00	$4.74(7)\cdot10^{-4}$	$1.89(3)\cdot10^{-3}$	$4.43(8)\cdot10^{-3}$	$1.19(10)\cdot10^{-2}$
1.00	$4.35(4)\cdot10^{-4}$	$1.78(3)\cdot10^{-3}$	$4.18(6)\cdot10^{-3}$	$1.27(9)\cdot10^{-2}$
0.50	$4.72(6)\cdot10^{-4}$	$1.76(2)\cdot10^{-3}$	$4.09(7)\cdot10^{-3}$	$1.14(7)\cdot10^{-2}$
0.10	$2.67(3)\cdot10^{-4}$	$1.14(2)\cdot10^{-3}$	$2.71(4)\cdot10^{-3}$	$6.80(4)\cdot10^{-3}$
0.05	$1.96(2)\cdot10^{-4}$	$7.35(7)\cdot10^{-4}$	$2.38(3)\cdot10^{-3}$	$5.78(3)\cdot10^{-3}$
		Cu–H$_2$**L**$^{\mathbf{6}}$		
[H$^+$]	25 °C	35 °C	45 °C	55 °C
4.89	$2.03(3)\cdot10^{-3}$	$5.02(1)\cdot10^{-3}$	$1.34(1)\cdot10^{-2}$	$2.32(2)\cdot10^{-2}$
4.00	$1.95(3)\cdot10^{-3}$	$5.20(1)\cdot10^{-3}$	$1.35(1)\cdot10^{-2}$	$2.34(2)\cdot10^{-2}$
3.00	$2.00(4)\cdot10^{-3}$	$5.23(1)\cdot10^{-3}$	$1.30(1)\cdot10^{-2}$	$2.15(2)\cdot10^{-2}$
2.00	$2.24(4)\cdot10^{-3}$	$5.04(1)\cdot10^{-3}$	$1.23(1)\cdot10^{-2}$	$2.31(2)\cdot10^{-2}$
1.00	$2.03(3)\cdot10^{-3}$	$4.51(1)\cdot10^{-3}$	$1.07(4)\cdot10^{-2}$	$2.05(2)\cdot10^{-2}$
0.50	$1.71(3)\cdot10^{-3}$	$3.86(1)\cdot10^{-3}$	$9.13(5)\cdot10^{-3}$	$1.76(2)\cdot10^{-2}$
0.10	$9.96(1)\cdot10^{-4}$	$2.37(4)\cdot10^{-3}$	$5.76(2)\cdot10^{-3}$	$1.38(1)\cdot10^{-2}$
0.05	$6.83(5)\cdot10^{-4}$	$2.06(4)\cdot10^{-3}$	$4.90(1)\cdot10^{-3}$	$1.22(1)\cdot10^{-2}$
		Cu–H$_3$**L**$^{\mathbf{7}}$		
[H$^+$]	25 °C	35 °C	45 °C	55 °C
4.89	$1.57(2)\cdot10^{-3}$	$4.79(1)\cdot10^{-3}$	$1.11(3)\cdot10^{-2}$	$2.18(2)\cdot10^{-2}$
4.00	$1.59(4)\cdot10^{-3}$	$4.76(1)\cdot10^{-3}$	$1.11(4)\cdot10^{-2}$	$2.17(2)\cdot10^{-2}$
3.00	$1.57(2)\cdot10^{-3}$	$4.82(1)\cdot10^{-3}$	$1.09(3)\cdot10^{-2}$	$2.25(2)\cdot10^{-2}$
2.00	$1.55(2)\cdot10^{-3}$	$4.78(1)\cdot10^{-3}$	$1.15(3)\cdot10^{-2}$	$2.21(2)\cdot10^{-2}$
1.00	$1.46(2)\cdot10^{-3}$	$4.32(1)\cdot10^{-3}$	$1.07(3)\cdot10^{-2}$	$2.01(2)\cdot10^{-2}$
0.50	$1.36(2)\cdot10^{-3}$	$4.15(1)\cdot10^{-3}$	$9.62(3)\cdot10^{-3}$	$2.13(2)\cdot10^{-2}$
0.10	$1.04(1)\cdot10^{-3}$	$3.39(1)\cdot10^{-3}$	$8.31(2)\cdot10^{-3}$	$1.68(1)\cdot10^{-2}$
0.05	$9.64(1)\cdot10^{-4}$	$2.65(1)\cdot10^{-3}$	$7.40(5)\cdot10^{-3}$	$1.58(1)\cdot10^{-2}$

[a] Conditions used: I = 5.0 M (H,Na)ClO$_4$.

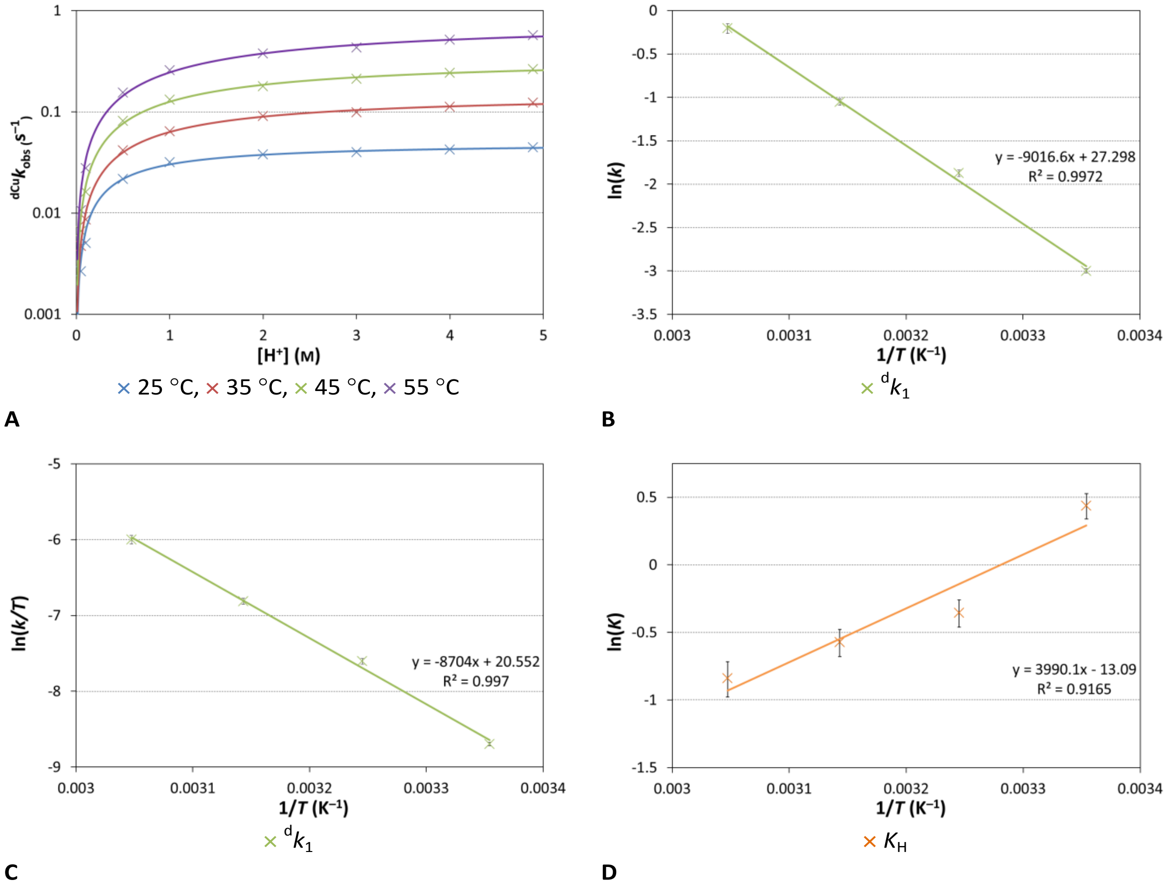

Figure S19. (A) Dependence of $^{d}k_{obs}$ of acid-assisted decomplexation of Cu(II)–**TMC** complex [25 °C, 35 °C, 45 °C and 55 °C, I = 5.0 M (H,Na)ClO$_4$]. (B) Linearized temperature dependence of $^{d}k_1$ according to Arrhenius equation. (C) Linearized temperature dependence of $^{d}k_1$ according to Eyring equation. (D) Linearized temperature dependence of K_H.

Table S6. Activation and thermodynamic parameters of rate and equilibrium constants associated with an acid-assisted dissociation of Cu(II)–**TMC** complex.

Temperature [°C]	Rate constant		Equilibrium constant	
	$^{d}k_1$ [s^{-1}]		K_H [mol^{-1}·dm^3]	logK_H
25	4.98(11)·10^{-2}		1.5(1)	0.18
35	1.5(1)·10^{-1}		7(1)·10^{-1}	–0.15
45	3.5(1)·10^{-1}		6(1)·10^{-1}	–0.25
55	8.1(5)·10^{-1}		4(1)·10^{-1}	–0.36
	Activation/thermodynamic parameters			
E_a [kJ mol^{-1}]^a	75(3)	ΔH^0 [kJ mol^{-1}]^c	–33(7)	
$\Delta H^\#$ [kJ mol^{-1}]^b	72(3)	ΔS^0 [J K^{-1} mol^{-1}]^c	–109(23)	
$\Delta S^\#$ [J K^{-1} mol^{-1}]^b	–27(9)			

^{a} $\ln k = -(E_a/RT) + \ln A$, ^{b} $\ln(k/T) = -(\Delta H^\#/RT) + (\Delta S^\#/R) + \ln(k_b/h)$, ^{c} $\ln K_H = -(\Delta H^0/RT) + (\Delta S^0/R)$

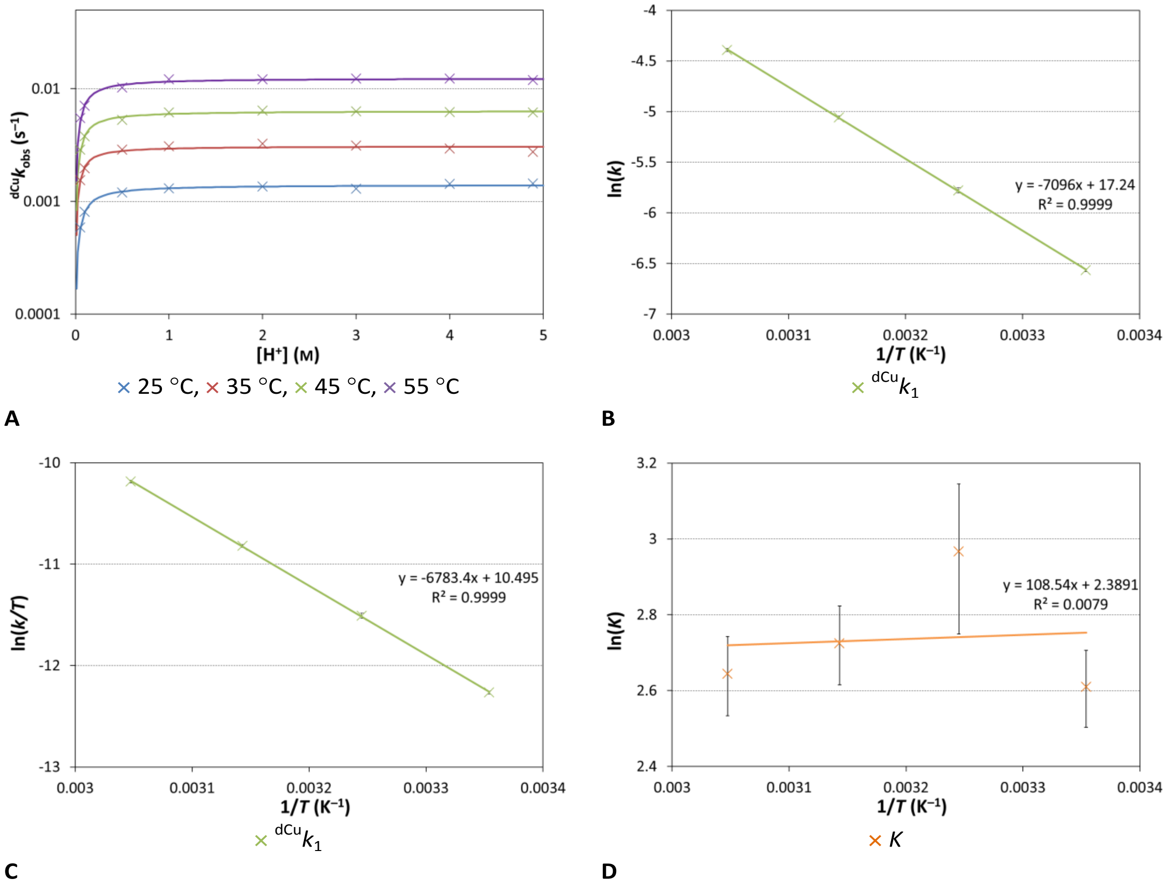

Figure S20. (A) Dependence of $^{d}k_{obs}$ of acid-assisted decomplexation of Cu(II)–H**L**^{1} complex [25 °C, 35 °C, 45 °C and 55 °C, I = 5.0 M (H,Na)ClO$_4$]. (B) Linearized temperature dependence of $^{d}k_1$ according to Arrhenius equation. (C) Linearized temperature dependence of $^{d}k_1$ according to Eyring equation. (D) Linearized temperature dependence of K_H.

Table S7. Activation and thermodynamic parameters of rate and equilibrium constants associated with an acid-assisted dissociation of Cu(II)–H**L**^{1} complex.

Temperature [°C]	Rate constant		Equilibrium constant	
	$^{d}k_1$ [s^{-1}]		K_H [mol^{-1}·dm^3]	logK_H
25	$1.41(2)\cdot10^{-3}$		14(1)	1.13
35	$3.1(1)\cdot10^{-3}$		19(4)	1.29
45	$6.4(1)\cdot10^{-3}$		15(2)	1.18
55	$1.24(2)\cdot10^{-2}$		14(2)	1.15
	Activation/thermodynamic parameters			
E_a [kJ mol^{-1}]^a	58.9(4)	ΔH^0 [kJ mol^{-1}]^c	–1(7)	
$\Delta H^\#$ [kJ mol^{-1}]^b	56.6(3)	ΔS^0 [J K^{-1} mol^{-1}]^c	20(23)	
$\Delta S^\#$ [J K^{-1} mol^{-1}]^b	–109.5(8)			

^{a} $\ln k = -(E_a/RT) + \ln A$, ^{b} $\ln(k/T) = -(\Delta H^\#/RT) + (\Delta S^\#/R) + \ln(k_b/h)$, ^{c} $\ln K_H = -(\Delta H^0/RT) + (\Delta S^0/R)$

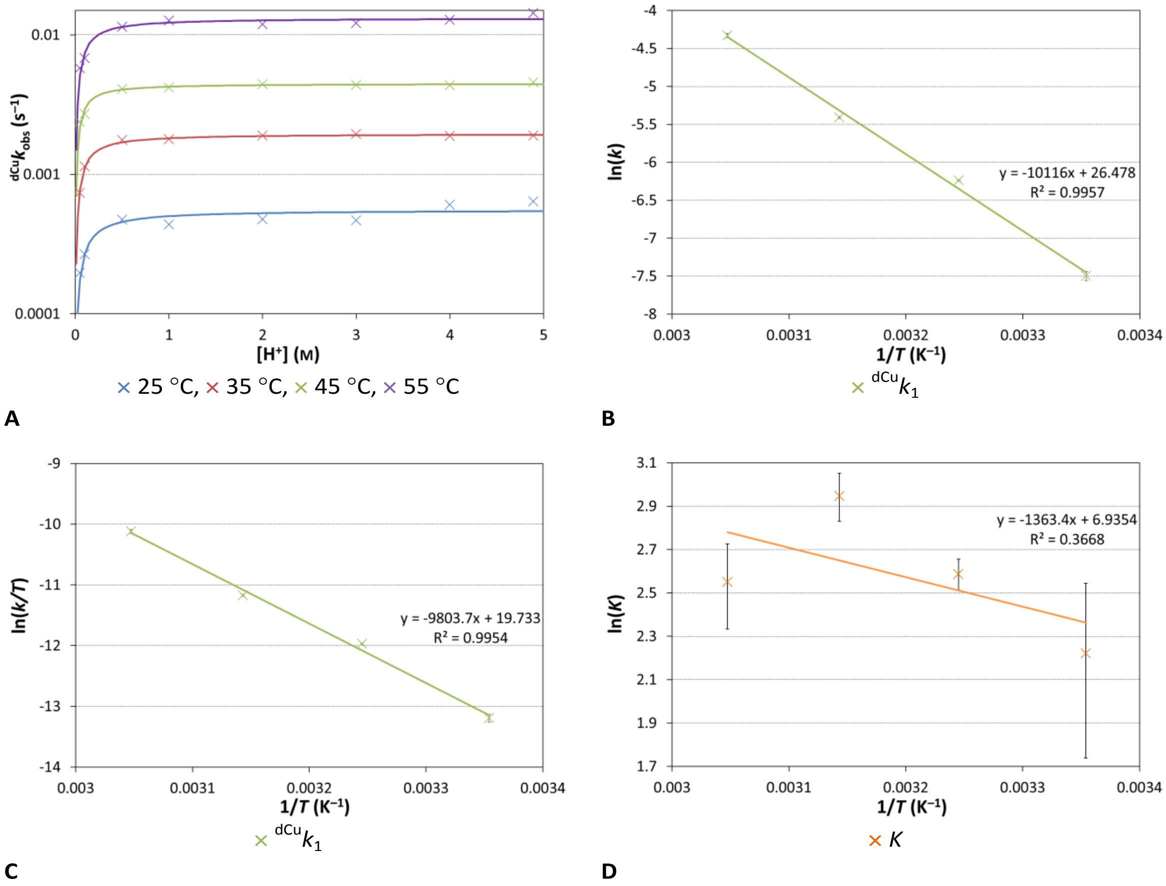

Figure S21. (A) Dependence of $^{d}k_{obs}$ of acid-assisted decomplexation of Cu(II)–H$_2$**L**^{3} complex [25 °C, 35 °C, 45 °C and 55 °C, I = 5.0 M (H,Na)ClO$_4$]. (B) Linearized temperature dependence of $^{d}k_1$ according to Arrhenius equation. (C) Linearized temperature dependence of $^{d}k_1$ according to Eyring equation. (D) Linearized temperature dependence of K_H.

Table S8. Activation and thermodynamic parameters of rate and equilibrium constants associated with an acid-assisted dissociation of Cu(II)–H$_2$**L**^{3} complex.

Temperature [°C]	Rate constant		Equilibrium constant	
	$^{d}k_1$ [s^{-1}]		K_H [mol^{-1}·dm^3]	logK_H
25	5.6(3)·10^{-4}		9(4)	0.96
35	1.95(2)·10^{-3}		13(1)	1.12
45	4.5(1)·10^{-3}		19(2)	1.28
55	1.32(4)·10^{-2}		13(4)	1.11
	Activation/thermodynamic parameters			
E_a [kJ mol^{-1}]^a	84(4)	ΔH^0 [kJ mol^{-1}]^c	11(11)	
$\Delta H^\#$ [kJ mol^{-1}]^b	82(4)	ΔS^0 [J K^{-1} mol^{-1}]^c	58(34)	
$\Delta S^\#$ [J K^{-1}·mol^{-1}]^b	−33(13)			

^{a} ln$k$ = −(E_a/RT) + ln$A$, ^{b} ln(k/T) = −($\Delta H^\#$/RT) + ($\Delta S^\#$/R) + ln(k_b/h), ^{c} lnK_H = −(ΔH^0/RT) + (ΔS^0/R)

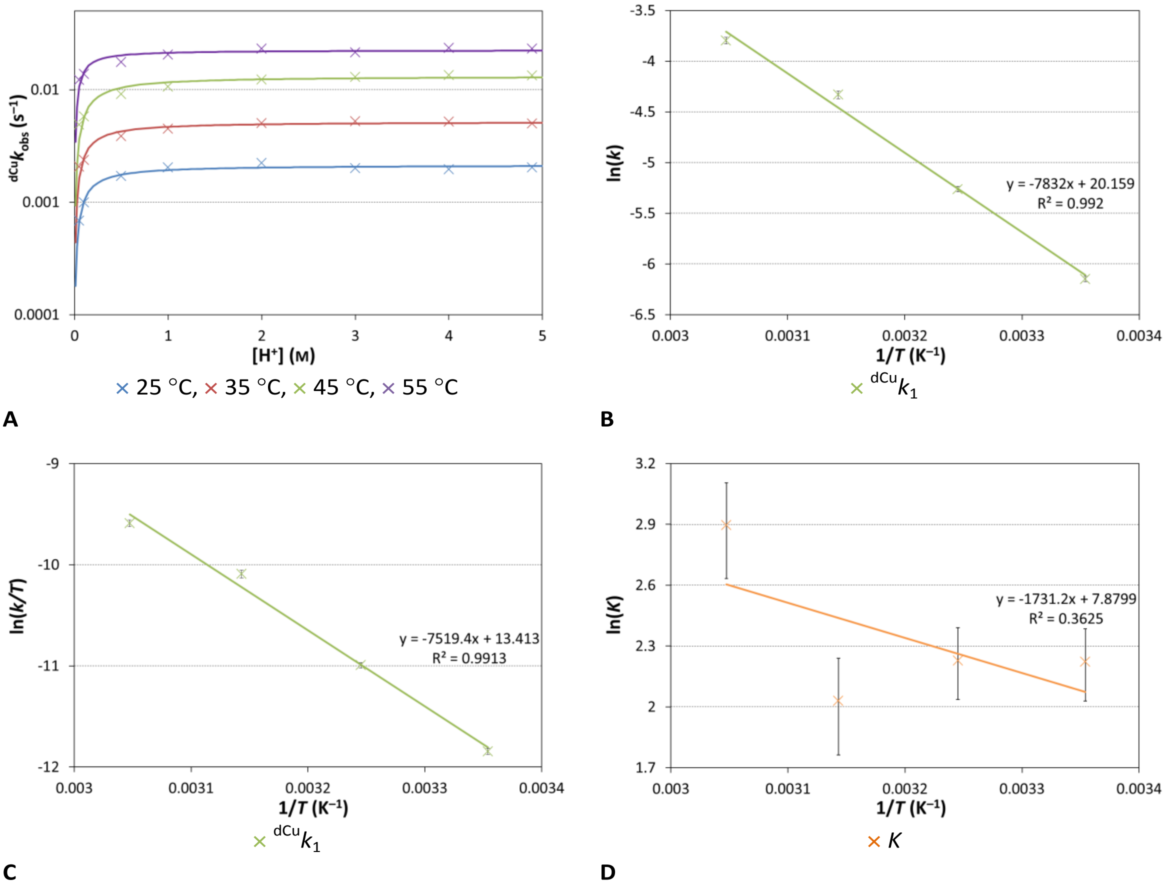

Figure S22. (A) Dependence of ${}^{d}k_{obs}$ of acid-assisted decomplexation of Cu(II)–H$_2$**L**^{6} complex [25 °C, 35 °C, 45 °C and 55 °C, I = 5.0 M (H,Na)ClO$_4$]. (B) Linearized temperature dependence of ${}^{d}k_1$ according to Arrhenius equation. (C) Linearized temperature dependence of ${}^{d}k_1$ according to Eyring equation. (D) Linearized temperature dependence of K_H.

Table S9. Activation and thermodynamic parameters of rate and equilibrium constants associated with an acid-assisted dissociation of Cu(II)–H$_2$**L**^{6} complex.

Temperature [°C]	Rate constant	Equilibrium constant	
	${}^{d}k_1$ [s^{-1}]	K_H [mol^{-1}·dm^3]	logK_H
25	2.1(1)·10^{-3}	9(2)	0.97
35	5.2(1)·10^{-3}	9(2)	0.97
45	1.3(1)·10^{-2}	8(2)	0.88
55	2.3(1)·10^{-2}	18(4)	1.26
	Activation/thermodynamic parameters		
E_a [kJ mol^{-1}]^a	65(4)	ΔH^0 [kJ mol^{-1}]^c	14(14)
$\Delta H^\#$ [kJ mol^{-1}]^b	63(4)	ΔS^0 [J K^{-1} mol^{-1}]^c	66(43)
$\Delta S^\#$ [J K^{-1} mol^{-1}]^b	−86(13)		

[a] $\ln k = -(E_a/RT) + \ln A$, [b] $\ln(k/T) = -(\Delta H^\#/RT) + (\Delta S^\#/R) + \ln(k_b/h)$, [c] $\ln K_H = -(\Delta H^0/RT) + (\Delta S^0/R)$

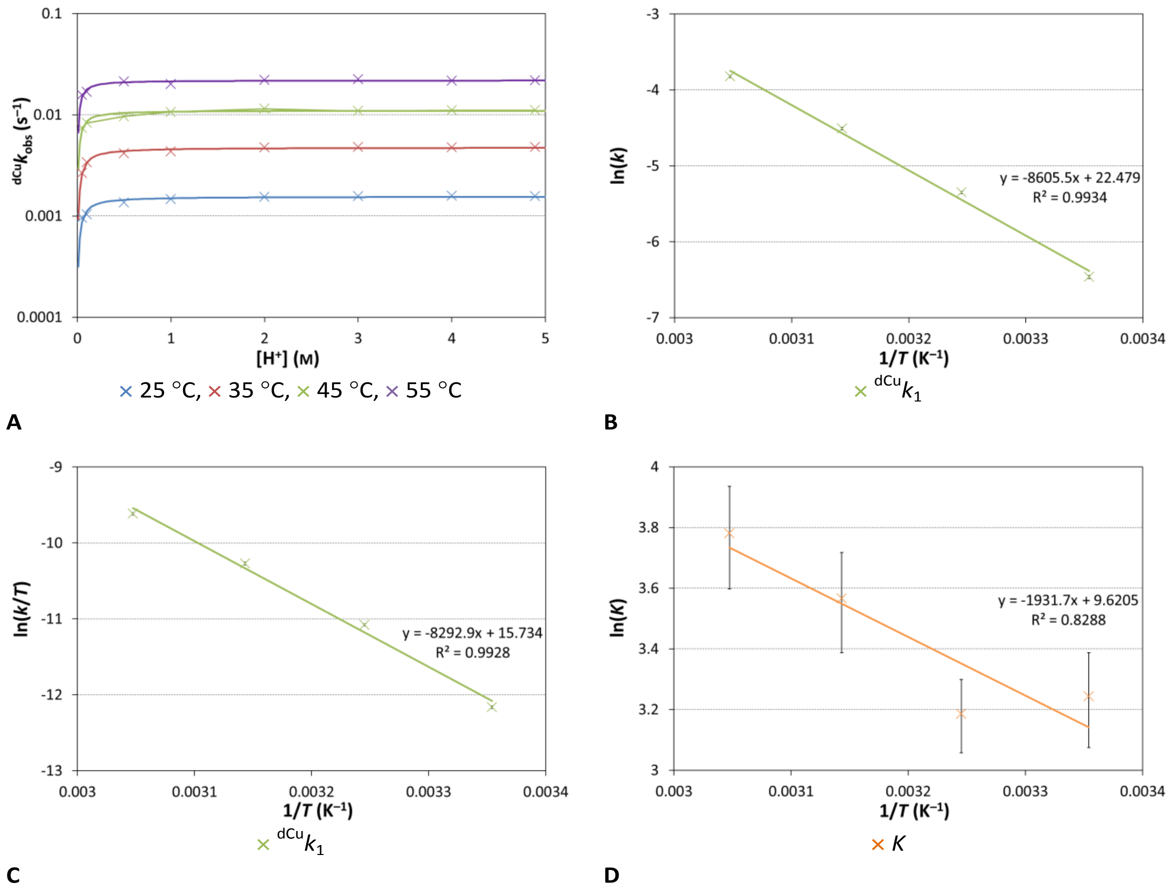

Figure S23. (A) Dependence of $^{d}k_{obs}$ of acid-assisted decomplexation of Cu(II)–H_3**L**^{7} complex [25 °C, 35 °C, 45 °C and 55 °C, I = 5.0 M (H,Na)ClO$_4$]. (B) Linearized temperature dependence of $^{d}k_1$ according to Arrhenius equation. (C) Linearized temperature dependence of $^{d}k_1$ according to Eyring equation. (D) Linearized temperature dependence of K_H.

Table S10. Activation and thermodynamic parameters of rate and equilibrium constants associated with an acid-assisted dissociation of Cu(II)–H_3**L**^{7} complex.

Temperature [°C]	Rate constant		Equilibrium constant	
	$^{d}k_1$ [s^{-1}]		K_H [mol^{-1}·dm^3]	logK_H
25	1.55(3)·10^{-3}		26(4)	1.41
35	4.8(1)·10^{-3}		24(3)	1.38
45	1.10(2)·10^{-2}		35(6)	1.55
55	2.20(4)·10^{-2}		44(7)	1.64
	Activation/thermodynamic parameters			
E_a [kJ mol^{-1}]^a	72(4)	ΔH^0 [kJ mol^{-1}]^c	16(5)	
$\Delta H^\#$ [kJ mol^{-1}]^b	69(4)	ΔS^0 [J K^{-1} mol^{-1}]^c	80(17)	
$\Delta S^\#$ [J K^{-1} mol^{-1}]^b	−67(13)			

^{a} $\ln k = -(E_a/RT) + \ln A$, ^{b} $\ln(k/T) = -(\Delta H^\#/RT) + (\Delta S^\#/R) + \ln(k_b/h)$, ^{c} $\ln K_H = -(\Delta H^0/RT) + (\Delta S^0/R)$

Detailed description of potentiometric experiments

The stock solutions of the ligands were prepared by dissolution of weighted material in a calibrated volumetric flask. The ligand concentration and hydrochloride content were determined by calculation of their concentration together with calculation of the ligand protonation constants. The calculated concentrations were consistent with those obtained by qNMR analysis used for determination of the synthetic yields. The stock solutions of the metal nitrates (recrystallized from deionized water) were standardized by titration with Na_2H_2edta according to the recommended procedure.[a] The stock solution of nitric acid ($c \approx 0.03$ м) was prepared from recrystallized KNO_3 on cation-exchange resin (Dowex 50). Carbonate-free KOH stock solution ($c \approx 0.2$ м) was standardized against potassium hydrogenphthalate and the HNO_3 solution was standardized against the stock KOH solution. The titrations were carried out in a vessel thermostated at 25±0.1 °C at ionic strength $I = 0.1$ м KNO_3 with addition of an excess of HNO_3 to the starting mixture. The inert atmosphere was ensured by a constant passage of argon saturated with water vapour. The ligand concentration in the titration vessel was ca. 0.004 м. The metal:ligand ratio was 1:1 in all cases. Stock solution of KOH was gradually added using a 2-ml ABU 900 automatic piston burette and the electrode potential was read using a PHM 240 pH-meter with GK 2401C/B combined electrode (all Radiometer). Before and after each titration, electrode calibration titrations (titration of standard HNO_3 with standard KOH solutions) were performed to determine calibration parameters and to check the stability of the electrode system during the experiments. From the calibration titrations, the parameters describing the electrode behaviour according to the calibration function $E = E_0 + S \cdot \log[H^+] + j_1 \cdot [H^+] + j_2 \cdot K_w/[H^+]$ were calculated, where the additive term E_0 contains the standard potential of the electrode used and contributions of inert ions to the liquid-junction potential, S corresponds to the Nernstian slope, the value of which should be close to the theoretical value, and $j_1 \cdot [H^+]$ and $j_2 \cdot K_w/[H^+]$ terms are the contributions of the H^+ and OH^- ions to the liquid-junction potential causing some deviations from a linear dependence of E on $\log[H^+]$ in strongly acid and strongly alkaline solutions, respectively.

The equilibria in H^+–ligand and H^+–Cu(II)–ligand systems were established fast and, thus, standard potentiometric titrations with starting volumes of ca. 5 cm^3 were used with waiting for equilibration for 20–60 s before reading electrode potential. Titrations were performed in pH range ca. 1.5–12 for Cu–H**L**^{1} system and 1.8–12 for other systems. The titrations of each system were carried out at least three times, each consisting of about 60 points.

Equilibria in solutions containing Ni(II) and Zn(II) ions were established slowly and, therefore, "out-of-cell" technique was used with initial volume of individual samples ca. 1 cm^3 and waiting time 3 weeks [H^+–Ni(II)–ligand systems] and 4 days [H^+–Zn(II)–ligand systems] to establish a full equilibrium. Then, potential at each titration point (tube) was determined with freshly calibrated electrode. Titrations were performed in pH range ca. 1.6–7 giving about 25 points for each of four independent titrations.

The constants with their standard deviations were calculated using the OPIUM program package.[b] Water ion product, $pK_w = 13.78$, and stability constants of M(II)–OH^- species were taken from the literature.[c] Calculated overall protonation constants are defined as $\beta_h = [H_hL]/\{[H]^h \cdot [L]\}$; they can be transferred to the consecutive protonation constants $\log K_h$ [$\log K_1 = \log\beta_1$ and in general $\log K_h(H_hL) = \log\beta_h - \log\beta_{(h-1)}$]. It should be noted that $\log K_h = pK_A$ of the corresponding protonated species. The stability constants β_{hlm} are defined as $\beta_{hlm} = [H_hL_lM_m]/\{[H]^h \cdot [L]^l \cdot [M]^m\}$ and could be converted to $\log K$ analogously as described above.

[a] R. Přibil, *Analytical Application of EDTA and Related Compounds*, Pergamon Press, Oxford, **1972**; G. Schwarzenbach and H. Flaschka, *Complexometric Titrations*, Methuen, London, **1969**.

[b] M. Kývala and I. Lukeš, *International Conference, Chemometrics '95*; Pardubice, Czech Republic, **1995**; p 63; full version of *OPIUM* software package is available (free of charge) on http://www.natur.cuni.cz/~kyvala/opium.html.

[c] C. F. Baes Jr. and R. E. Mesmer, *The Hydrolysis of Cations*, Wiley, New York, **1976**.

Table S11. Overall protonation constants ($\log\beta_h$)^a of the selected ligands obtained by potentiometry.^{b}

	h				
ligand	1	2	3	4	5
H**L**^{1}	10.59(1)	20.44(1)	22.97(1)	24.55(1)	–
H_2**L**^{3}	11.34(1)	22.09(1)	28.13(1)	30.81(2)	–
H**L**^{4}	10.13(1)	19.51(1)	22.31(1)	–	–
H_3**L**^{7}	11.47(1)	21.88(1)	29.50(1)	33.13(2)	34.64(2)

^{a} $\beta_h = [H_hL]/\{[H]^h \cdot [L]\}$. ^{b} Conditions used: $t = 25$ °C, $I = 0.1$ м KNO_3.

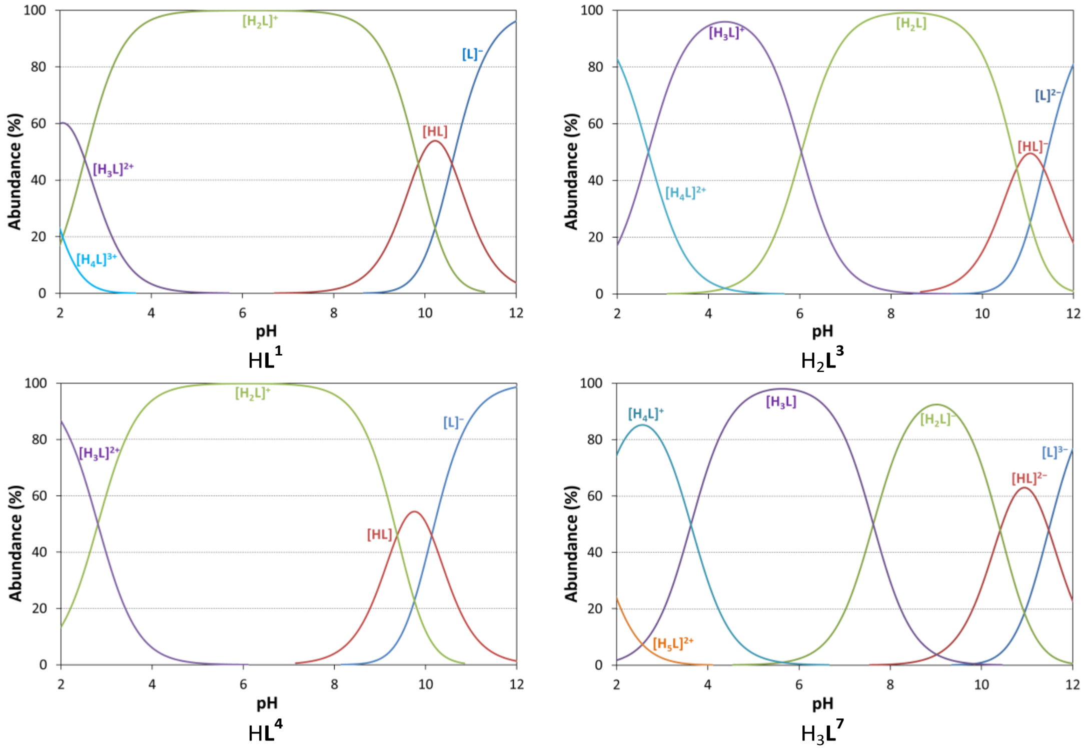

H**L**^{1} H$_2$**L**^{3} H**L**^{4} H$_3$**L**^{7}

Figure S24. Distribution diagrams of the selected ligands (protonation constants obtained by potentiometry, c_L = 0.004 м, t = 25 °C, I = 0.1 м KNO_3).

Table S12. Overall stability constants (logβ_{hlm})[a] of complexes of the selected ligands with Cu(II), Ni(II) and Zn(II).[b]

h	l	m	H**L**^{1}	H$_2$**L**^{3}	H**L**^{4}	H$_3$**L**^{7}
				Cu^{2+}		
0	1	1	22.33(7)	22.26(5)	19.17(1)	23.00(3)
1	1	1	–	27.75(3)	–	30.37(1)
				Ni^{2+}		
0	1	1	15.05(4)	15.84(5)	11.73(8)	14.75(3)
1	1	1	–	–	–	21.75(2)
				Zn^{2+}		
0	1	1	15.16(3)	17.75(3)	13.03(9)	16.05(5)
1	1	1	–	22.41(5)	–	23.21(2)

[a] $\beta_{hlm} = [H_hL_lM_m]/\{[H]^h \cdot [L]^l \cdot [M]^m\}$. [b] Conditions used: t = 25 °C, I = 0.1 м KNO_3.

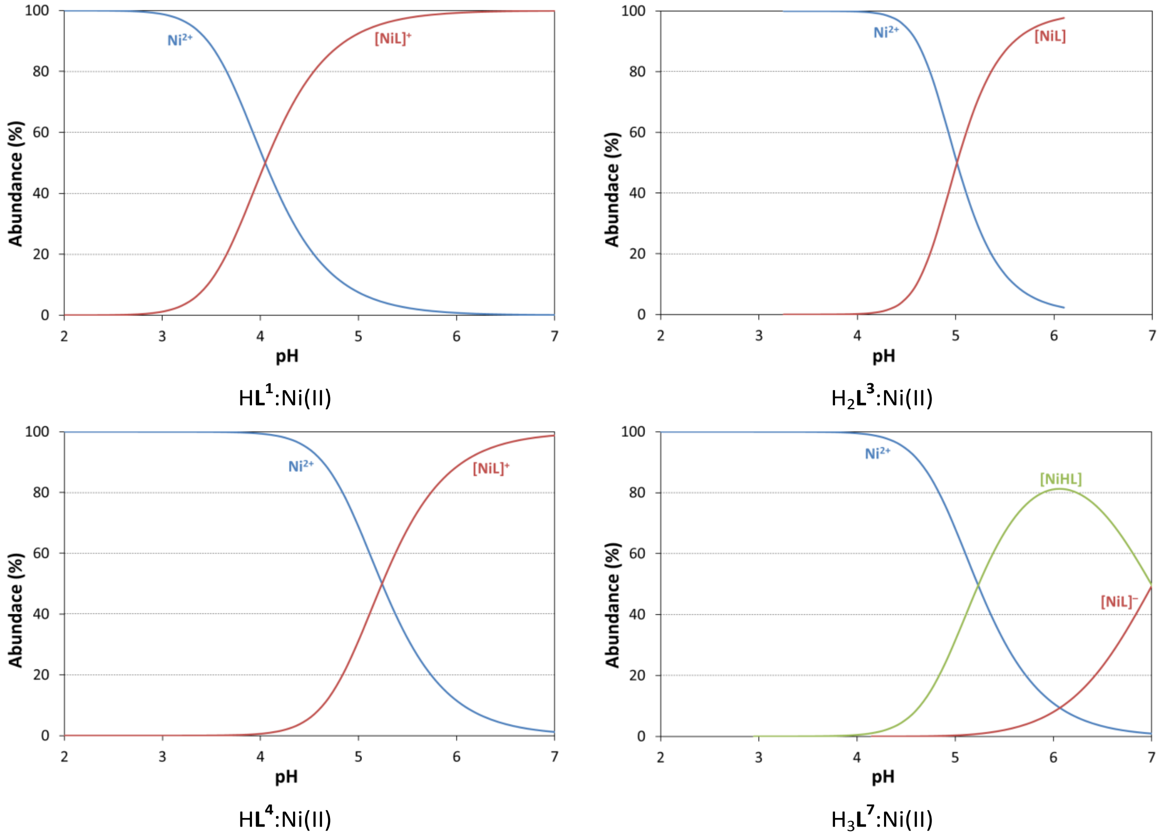

HL**¹**:Ni(II) H$_2$L**³**:Ni(II)

HL**⁴**:Ni(II) H$_3$L**⁷**:Ni(II)

Figure S25. Distribution diagrams of the metal-containing species in the Ni(II)–ligand systems ($c_L = c_M$ = 0.004 M, t = 25 °C, I = 0.1 M KNO_3).

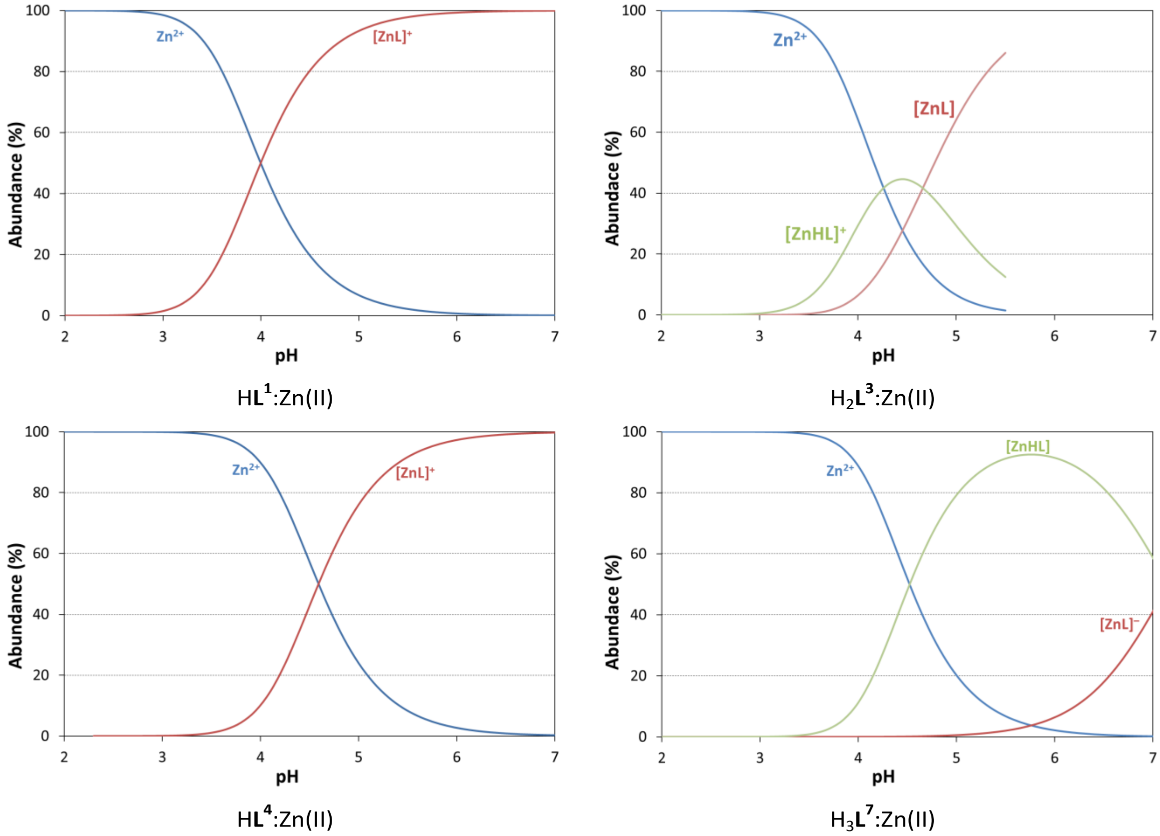

HL**¹**:Zn(II) H$_2$L**³**:Zn(II)

HL**⁴**:Zn(II) H$_3$L**⁷**:Zn(II)

Figure S26. Distribution diagrams of the metal-containing species in the Zn(II)–ligand systems ($c_L = c_M$ = 0.004 M, t = 25 °C, I = 0.1 M KNO_3).

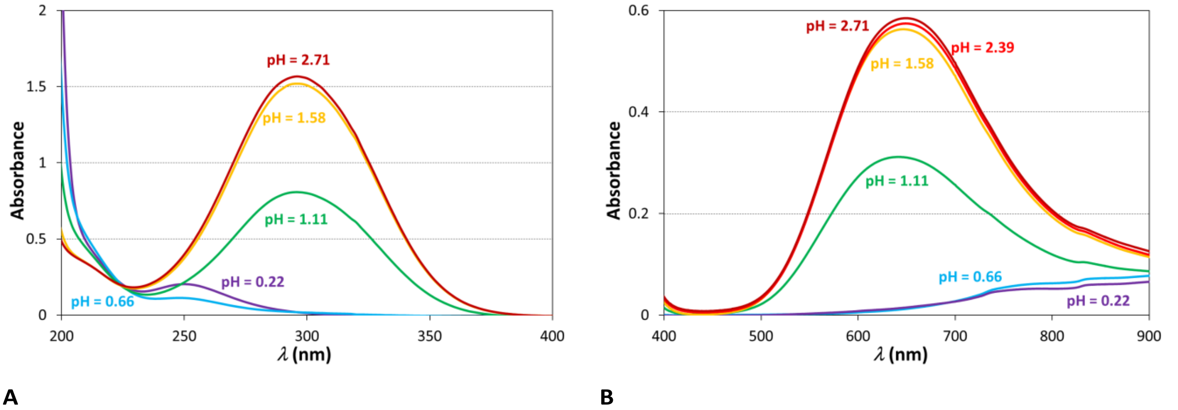

Figure S27. Course of selected UV-Vis spectra of Cu(II)–H**L**^{1} system with increasing pH ($c_L = c_M$ = 0.0026 M, t = 25 °C, no control of ionic strength). (A) LM-CT band, 1mm cuvette. (B) d-d transition band, 10mm cuvette.

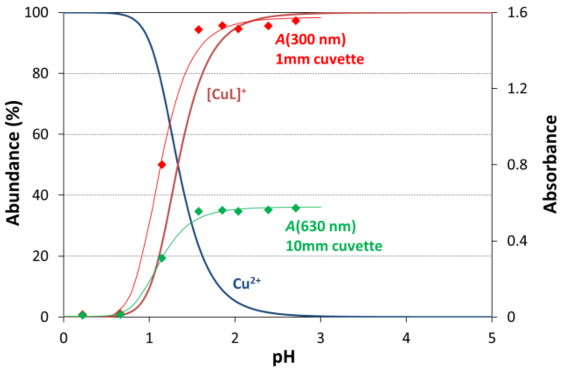

Figure S28. Overlay of pH-dependence of absorbance at maxima of LM-CT band (300 nm, red diamonds) and d-d transition band (630 nm, green diamonds) with speciation diagram calculated from potentiometric results for Cu(II)–H**L**^{1} system. Thin red and green lines show the best fits of the UV-Vis spectral data.

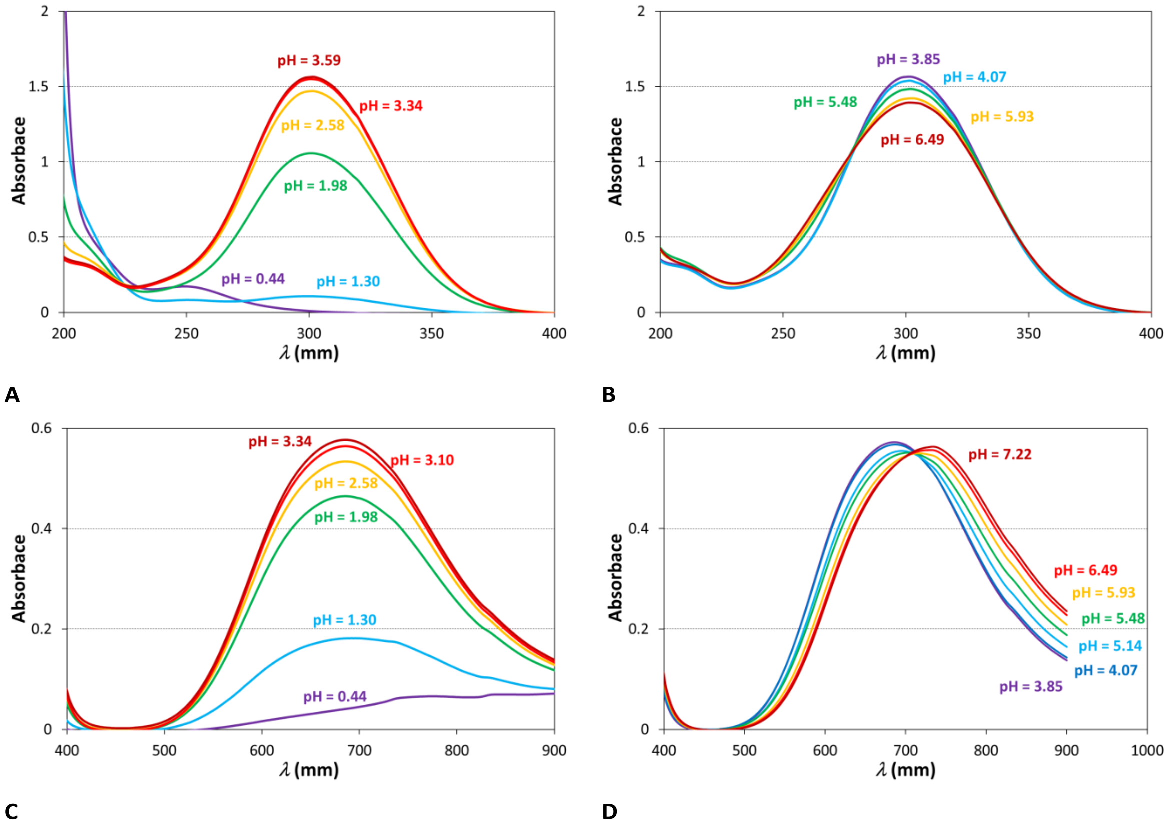

Figure S29. Course of selected UV-Vis spectra of Cu(II)–$H_2\mathbf{L}^3$ system with increasing pH (c_L = c_M = 0.0026 M, *t* = 25 °C, no control of ionic strength). (A) LM-CT band, 1mm cuvette, strong acid region. (B) LM-CT band, 1mm cuvette, weak acid to neutral region. (C) d-d transition band, 10mm cuvette, strong acid region. (D) d-d transition band, 10mm cuvette, weak acid to neutral region.

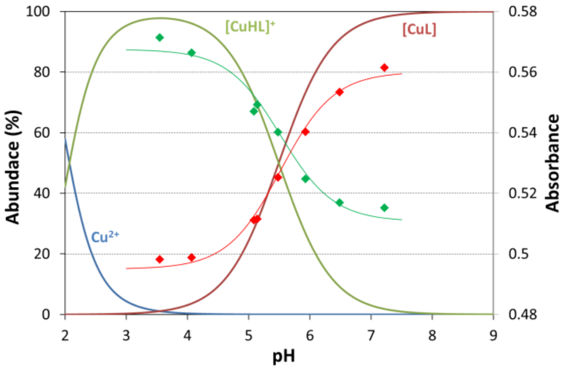

Figure S30. Overlay of pH-dependence of absorbance at maxima of d-d transition bands (680 nm, green diamonds; 740 nm, red diamonds) with speciation diagram calculated from potentiometric results for Cu(II)–$H_2\mathbf{L}^3$ system. Thin red and green lines show the best fits of the UV-Vis spectral data.

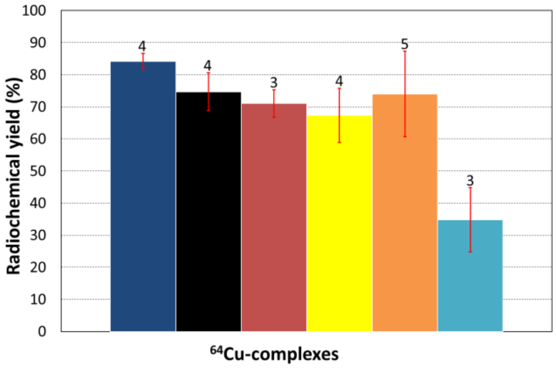

Figure S31. Graphical representation of radiochemical yield (%) of ^{64}Cu(II) complexes at pH = 6.2 (MES buffer). Error bars show a data-spreading, the numbers indicate a number of independent batches of ^{64}Cu used for complexation experiments. The molar ratio ^{64}Cu:ligand ≈ 1:100, 25 °C, 10 min.